Prediction of octanol-water partition coefficients for the SAMPL6-logP molecules using molecular dynamics simulations with OPLS-AA, AMBER and CHARMM force fields

Shujie Fan, Bogdan Iorga, Oliver Beckstein

Journal of Computer-Aided Molecular Design manuscript No.
(will be inserted by the editor)

Prediction of octanol-water partition coefficients for the SAMPL6-log P molecules using molecular dynamics simulations with OPLS-AA, AMBER and CHARMM force fields

Shujie Fan · Bogdan I. Iorga · Oliver Beckstein

Received: 16 October 2019 / Accepted: 27 November 2019

Abstract All-atom molecular dynamics simulations with stratified alchemical free energy calculations were used to predict the octanol-water partition coefficient $\log P_{ow}$ of eleven small molecules as part of the SAMPL6-log P blind prediction challenge using four different force field parametrizations: standard OPLS-AA with transferable charges, OPLS-AA with non-transferable CM1A charges, AMBER/GAFF, and CHARMM/CGenFF. Octanol parameters for OPLS-AA, GAFF and CHARMM were validated by comparing the density as a function of temperature to experimental values. The partition coefficients were calculated from the solvation free energy for the compounds in water and pure ("dry") octanol or "wet" octanol with 27 mol % water dissolved. Absolute solvation free energies were computed by thermodynamic integration (TI) and the Multistate Bennett Acceptance Ratio (MBAR) with uncorrelated samples from data generated by an established protocol using 5-ns windowed alchemical free energy perturbation (FEP) calculations with the Gromacs molecular

Research reported in this publication was supported by the National Institute Of General Medical Sciences of the National Institutes of Health under Awards Number R01GM118772 and R01GM125081. BII was supported in part by grants ANR-10-LABX-33 (LabEx LERMIT) and ANR-14-JAMR-0002-03 (JPIAMR) from the French National Research Agency (ANR), and by a grant DIM MAL-INF from the Région Ile-de-France.

S. Fan
Department of Physics, Arizona State University, P.O. Box 871504, Tempe, AZ 85287-1504, USA

B. I. Iorga
Institut de Chimie des Substances Naturelles, CNRS UPR 2301, Université Paris-Saclay, Labex LERMIT, 1 Avenue de la Terrasse, 91198 Gif-sur-Yvette, France
Tel.: +33 1 69 82 30 94
Fax: +33 1 69 07 72 47
E-mail: bogdan.iorga@cnrs.fr

O. Beckstein
Department of Physics and Center for Biological Physics, Arizona State University, P.O. Box 871504, Tempe, AZ 85287-1504, USA
Tel.: +1 480 727 9765
Fax: +1 480 965-4669
E-mail: oliver.beckstein@asu.edu

dynamics package. Equilibration of sets of FEP simulations was quantified by a new measure of convergence based on the analysis of forward and time-reversed trajectories. The accuracy of the $\log P_{ow}$ predictions was assessed by descriptive statistical measures such as the root mean square error (RMSE) of the data set compared to the experimental values. Discarding the first 1 ns of each 5-ns window as an equilibration phase had a large effect on the GAFF data, where it improved the RMSE by up to 0.8 log units, while the effect for other data sets was smaller or marginally worsened the agreement. Overall, CGenFF gave the best prediction with RMSE 1.2 log units, although for only eight molecules because the current CGenFF workflow for Gromacs does not generate files for certain halogen-containing compounds. Over all eleven compounds, GAFF gave an RMSE of 1.5. The effect of using a mixed water/octanol solvent slightly decreased the accuracy for CGenFF and GAFF and slightly increased it for OPLS-AA. The GAFF and OPLS-AA results displayed a systematic error where molecules were too hydrophobic whereas CGenFF appeared to be more balanced, at least on this small data set.

Keywords molecular dynamics · solvation free energy · OPLS-AA force field · AMBER force field · CHARMM force field · ligand parametrization · free energy perturbation · octanol-water partition coefficient

1 Introduction

One key consideration in the design of small-molecule drugs is to enable these molecules to efficiently reach their site of action, which typically requires the crossing of the lipid bilayer of the cell membrane such as in the epithelial lining of the gut or the blood-brain barrier. Although in some cases active transport processes are co-opted for drug transport [1], passive diffusion across the cell membrane remains the primary route for drug absorption [2]. The ability of a molecule to partition into the water or the lipid phase can be assessed by its water-octanol partition coefficient P_{ow} (or its decadic logarithm $\log P_{ow}$, often just written as "logP") where octanol is taken as a simple approximation to the lipid membrane. A $\log P_{ow} < 0$ indicates a hydrophilic molecule, $\log P_{ow} \approx 0$ indicates equal distribution in water and octanol phase, and $\log P_{ow} > 0$ indicates lipophilicity. The $\log P_{ow}$ value is one of the quantities in the "rule of five" guidelines to assess drug permeability [3], where $\log P_{ow} > 5$ is indicative of poor drug solubility and permeability (in conjunction with more than 5 hydrogen-bond donors/2×5 acceptors, and a molecular weight greater than 500).

Partition coefficients are physico-chemical quantities that are, in principle, straightforward to calculate with physics-based simulation approaches from the solvation free energies of the solute in the two solvents (ΔG_w in water and ΔG_o in octanol)

$$\log P_{ow} = (\Delta G_w - \Delta G_o)(RT)^{-1} \log e, \tag{1}$$

where $R = 8.31446261815 \times 10^{-3}\,\mathrm{kJ \cdot mol^{-1} \cdot K^{-1}}$ is the universal Gas constant (i.e., Boltzmann's constant for 1 mol), T is the temperature, and e Euler's number. Calculation of partition coefficients requires (1) accurate representation of the interactions between solvent and solute, (2) proper representation of the solute structure

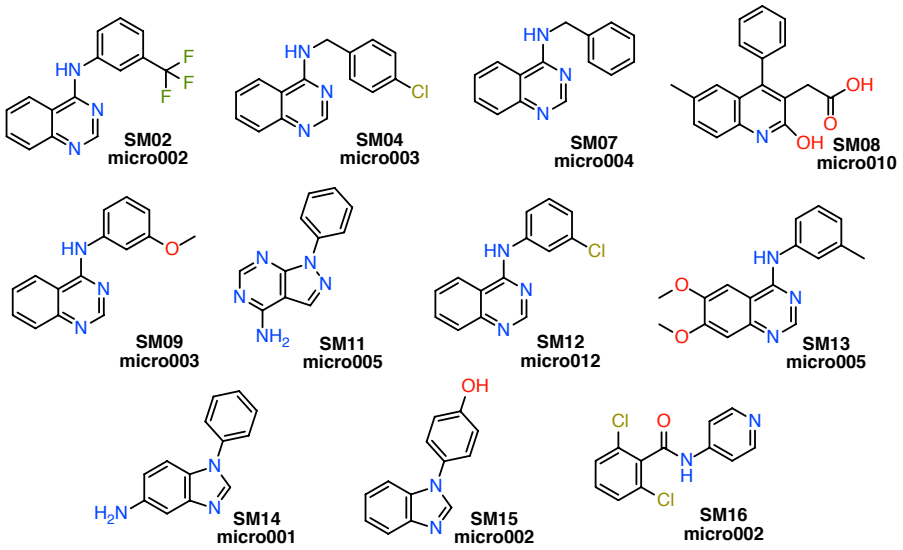

Fig. 1: Chemical structures of the SAMPL6-logP data set with the selected microstates.

(tautomers) and (3) correct sampling of the thermodynamic equilibrium. Therefore, they make for good benchmark systems to assess the current state of the art in predictive free energy calculations, as evidenced by the 2016 SAMPL5 challenge on cyclohexane partition coefficients [4] and the 2019 SAMPL6 challenge on the water-octanol partition coefficients. The chemical structures of compounds included in the SAMPL6-logP data set are shown in Figure 1. The logP values of the compounds were measured by the organizers and had not been previously published [5]; participants submitted blind predictions for evaluation against the experimental values.

For the SAMPL6 challenge we used the same approach as for previous solvation-free energy based challenges [6–8], namely classical molecular dynamics (MD) with explicit solvent. We evaluated three widely used force fields, OPLS-AA, AMBER/GAFF, and CHARMM/CGenFF. For all three force fields reasonably user-friendly parametrization tools exist and we wondered what performance a user could expect from just using these tools. Additionally, we also used the same in-house approach to generate OPLS-AA topologies that we had employed in previous challenges [6–8].

2 Methods

Our computational approach to calculating solvation free energies with classical MD and our MDPOW Python package (`https://github.com/Becksteinlab/mdpow/`) is similar to our previous SAMPL contributions [6–8]. Nevertheless, we will describe the details for completeness together with improvements that resulted from lessons that we learned during this challenge. Previously, we only evaluated OPLS-

AA parametrizations but for this challenge we also evaluated additional force fields (AMBER and CHARMM) with the same protocol.

2.1 Force field parameters

Molecules included in the SAMPL6-log$P$ data set (Figure 1) were parameterized with different force fields, as detailed below. Three-dimensional coordinates for molecules included in this study were obtained from our participation [9] in the SAMPL6 pK_a prediction challenge [10], the gas-phase geometry optimization being performed with GAUSSIAN09 version D.01 [11] at the B3LYP/6-311+G(d,p) level.

The OPLS-AA [12–18] parameters for these compounds were generated either with transferable charges using our in house MOL2FF algorithm (O. Beckstein and B. I. Iorga, unpublished), based on the CACTVS Chemoinformatics Toolkit (`http://www.xemistry.com/`), or with CM1A charges (scaled with a factor of 1.14 for neutral molecules) using the LigParGen web server [19] (`http://zarbi.chem.yale.edu/ligpargen/`)

The parameters of SAMPL6-logP compounds for the CHARMM/CGenFF force field [20] were obtained from the CGenFF server (`https://cgenff.umaryland.edu/`) using the CGenFF program version 2.2.0 and CGenFF 4.0 [21, 22] with mol2 files as inputs. The resulting CHARMM files were converted to Gromacs files with the Python script `cgenff_charmm2gmx.py` (downloaded from `http://mackerell.umaryland.edu/download.php?filename=CHARMM_ff_params_files/cgenff_charmm2gmx.py`, copyright notice from 2014). This version of the conversion script cannot correctly process recent CGenFF parameters for lone pairs to represent compounds with certain halogen substituents [23]. Because compounds **SM04**, **SM12** and **SM16** contained halogens with lone pairs, we were not able to obtain CGenFF parameters in the Gromacs format and could not include them in the CGenFF results. Although it is possible to manually fix topologies and represent the lone pairs with Gromacs virtual site constructs, we decided against doing so as the average user would likely not be able to perform such topology hacking; furthermore, such functionality should be automated and tested in the conversion script and not performed on a case-by-case basis in order to aid reproducibility and applicability to large data sets.

The AMBER/GAFF [24] parameters for the SAMPL6-logP data set were generated with AM1-BCC charges using AmberTools15 (`http://ambermd.org`) with version 1.4 of GAFF and ACPYPE [25].

The OPLS-AA hydration free energies simulations were performed using the TIP4P water model [26] and those using CHARMM36 [27] and AMBER99sb [28] force fields were carried out using the TIP3P water model [29], which are the water models used for the development of the corresponding force fields, respectively. For simulations with octanol, we generated parameters for this solvent molecule for OPLS-AA with MOL2FF, for GAFF with AmberTools17, and for CGenFF with the CGenFF server, and tested them with simulations of bulk octanol, as described in Results (Section 3.1).

Besides the pure octanol solvent, we decided to use a water-octanol mixture for solvation free energy calculations, as the experimental octanol-water partition coefficients were measured in a way that the water and octanol phases might not be pure water and octanol. The solubility of octanol in water is very low [30–32] so we only considered pure water phases. On the other hand, the equilibrium solubility of water in octanol at room temperature (298 K) is about 5 mass % [30–32]. Hence we also prepared a mixed solvent water-octanol ("wet" octanol) box with a mole fraction of water in octanol of 27 mol % and performed octanol solvation free energy calculations with either the pure octanol solvent (*dry*) or the *wet* octanol.

2.2 Solvation free energy and partition coefficient calculation

Solvation free energies were calculated as described previously [8] via stratified all-atom alchemical free energy perturbation (FEP) MD simulations. All simulations were performed with the MDPOW Python package (`https://github.com/Becksteinlab/mdpow/`, 0.7.0 development version) with Gromacs 2018.2 [33] as its MD engine. Autocorrelation analysis, thermodynamic integration (TI), and the multistate Bennett acceptance ratio (MBAR) [34] were performed with the ALCHEMLYB Python package (`https://github.com/alchemistry/alchemlyb`), release 0.3.0 [35].

A periodic cubic simulation cell was employed with at least 1.5 nm between the solute and the box surfaces. The simulations were run as Langevin dynamics (integration time step 2 fs) for temperature control, with the friction coefficient for each particle computed as mass/0.1 ps [36]. All simulations were run in the *NPT* ensemble, and the average pressure was maintained near the target value 1 bar with an isotropic pressure Parinello-Rahman barostat [37] with relaxation time constant $\tau_p =$ 1 ps and compressibility $\kappa_T = 4.6 \times 10^{-5}$ bar^{-1} for both water and octanol. Lennard-Jones interactions were calculated up to a cutoff of 1 nm without force-switching for OPLS-AA and AMBER simulations and a cutoff of 1.2 nm with a force-switching cutoff of 1.0 nm for CHARMM simulations, and a dispersion correction was applied to energy and pressure to account for van der Waals interactions beyond the cutoff in a mean field manner [38] for OPLS-AA and AMBER. Coulomb interactions were evaluated with the SPME method [39] with an initial short range cutoff of 1 nm, 0.12 nm Fourier grid spacing, sixth order spline interpolation, and a relative tolerance of 10^{-6}. Each simulation was run on six CPU cores and a single GPU and Gromacs was allowed to tune the Coulomb short range cut-off to optimize performance. All bonds containing hydrogen atoms were constrained with the P-LINCS algorithm [40] using a twelfth order expansion with a single iteration.

Solvated systems were energy minimized and relaxed with a *NPT* MD simulation with a time step of 0.1 fs and duration of 5 ps. An initial *NPT* equilibrium simulation at constant temperature and pressure ($T = 300$ K, $P = 1$ bar) was carried out for 15 ns. The last frame of the equilibrium simulation served as the starting configuration for the windowed FEP calculations. The FEP calculations were also carried out in the *NPT* ensemble. Coulomb interactions (partial charges) were linearly switched off over five windows (coupling parameter $\lambda_{\mathrm{Coul}} \in \{0, 0.25, 0.5, 0.75, 1\}$) for water

simulations, and seven windows (coupling parameter $\lambda_{\text{Coul}} \in \{0, 0.125, 0.25, 0.375, 0.5, 0.75, 1\}$) for dry octanol or wet octanol simulations, while the van der Waals (Lennard-Jones) interactions were maintained (i.e. $\lambda_{\text{vdW}} = 0$); sixteen windows were used to switch off the Lennard-Jones term for the uncharged solute ($\lambda_{\text{Coul}} = 1$ and $\lambda_{\text{vdW}} \in \{0, 0.05, 0.1, 0.2, 0.3, 0.4, 0.5, 0.6, 0.65, 0.7, 0.75, 0.8, 0.85, 0.9, 0.95, 1\}$). Each window was simulated for 5 ns. The van der Waals calculations used soft core potentials with the values suggested by Mobley and colleagues [36] ($\alpha = 0.5$, power 1, and $\sigma = 0.3$ nm). The calculations made use of the "`couple-intramol = no`" feature in Gromacs [33, 41, 42], which maintains intramolecular interactions while decoupling all intermolecular ones.

Autocorrelation analysis was applied to the simulation data to obtain uncorrelated samples of the derivative of the Hamiltonian $\mathscr{H}$ with respect to the coupling parameter λ, $\partial\mathscr{H}/\partial\lambda$, and energy differences $\Delta U_{\text{i,j}}$ [43, 44]. For a time series of N samples, the autocorrelation function of the observable A at a given time frame i was defined as

$$C_i = \frac{\langle A_n A_{n+i}\rangle - \langle A_n\rangle^2}{\langle A_n^2\rangle - \langle A_n\rangle^2} \tag{2}$$

The integrated autocorrelation time τ_{ac} and statistical inefficiency g were given by

$$\tau_{ac} = \sum_{i=1}^{N}\left(1 - \frac{1}{N}\right) C_i \tag{3}$$

$$g = 1 + 2\tau_{ac} \tag{4}$$

Once the statistical inefficiency was found, every gth sample of the original data set was selected to build up a set of uncorrelated samples. In practice, we used $\partial\mathscr{H}/\partial\lambda$ as the observable A. Solvation free energies and statistical errors for the discharging and decoupling process were originally calculated with thermodynamic integration

$$\Delta G = \int_0^1 \left\langle \frac{\partial\mathscr{H}}{\partial\lambda}\right\rangle_\lambda d\lambda, \tag{5}$$

where the derivative of the Hamiltonian $\mathscr{H}$ with respect to the coupling parameter λ, $\partial\mathscr{H}/\partial\lambda$, was saved for every time step. In the MDPOW implementation of TI, Eq. 5 was integrated numerically with the composite Simpson's rule [45] from SciPy (`http://www.scipy.org`) [46]. The error on ΔG was calculated by propagating the errors of the individual $\langle\partial\mathscr{H}/\partial\lambda\rangle$ FEP windows through Simpson's rule as described previously [6]. The TI implementation of ALCHEMLYB uses the trapezoid rule and provides appropriate error estimates for uncorrelated data points. The ALCHEMLYB library provides the MBAR estimator [34], which also requires uncorrelated data for uncertainty estimates. We compared all three estimators and found that they generally agreed with each other. The final results shown in this paper were calculated with uncorrelated samples and the MBAR estimator [34].

The total solvation free energy (transfer from gas phase to aqueous phase at the 1M/1M Ben-Naim standard state)

$$\Delta G_{\text{solv}} = -(\Delta G_{\text{Coul}} + \Delta G_{\text{vdW}}) \tag{6}$$

was calculated as the sum of the Coulomb and van der Waals contributions, with the minus sign originating from the convention in Gromacs that $\lambda = 0$ corresponds to the fully coupled (solvated) state while $\lambda = 1$ describes a fully decoupled (gas-phase) solute.

In principle, the partition coefficient contains contributions from multiple tautomers with significant populations. To simplify the calculations, we only picked a single tautomer, typically with the lowest quantum mechanical ground state energy [9] and neutral overall charge, and calculated the octanol-water partition coefficients $\log P_{ow}$, Eq. 1, for one fixed state of the compound via the solvation free energies (Eq. 6).

2.3 Error analysis

As described previously [8], the error ε on $\log P_{ow}$ was calculated by error propagation from the errors of the individual free energies in Eq. 1 as

$$\varepsilon = \sqrt{\varepsilon_{\Delta G_o}^2 + \varepsilon_{\Delta G_w}^2}(RT)^{-1}\log_{10} e. \tag{7}$$

The difference between experimental and computed octanol-water coefficients ("signed error") for each of the N compounds, labeled with its identification code $\alpha = \mathbf{SM02}, \mathbf{SM04}, \ldots$, was calculated as

$$\Delta_\alpha = \log P_{ow,\alpha}, -\log P_{ow,\alpha}^{\text{exp}} \tag{8a}$$

$$\varepsilon_{\Delta,\alpha} = \sqrt{(\varepsilon_\alpha^2 + \varepsilon_\alpha^{\text{exp}})^2}, \tag{8b}$$

with the uncertainty ε_Δ of Δ determined as the standard error from propagating the experimental and simulation errors (Eq. 7) through Eq. 8a. The root mean square error (RMSE) was determined from the individual errors Δ as

$$\text{RMSE} = \sqrt{\langle \Delta^2 \rangle} = \sqrt{N^{-1}\sum_\alpha \Delta_\alpha^2}, \tag{9}$$

the absolute unsigned error (AUE) as

$$\text{AUE} = \langle |\Delta| \rangle = N^{-1}\sum_\alpha |\Delta_\alpha|\,, \tag{10}$$

and the signed mean error (ME, also called the "mean signed error", MSE) as

$$\text{ME} = \langle \Delta \rangle = N^{-1}\sum_\alpha \Delta_\alpha. \tag{11}$$

The standard errors of the RMSE, AUE, and ME were estimated via error propagation of the individual uncertainties Eq. 8b through Eqs. 9–11 as

$$\varepsilon_{\text{RMSE}} = \frac{1}{N\,\text{RMSE}}\sqrt{\sum_\alpha \Delta_\alpha^2 \varepsilon_{\Delta,\alpha}^2} = \frac{1}{\sqrt{N}}\sqrt{\frac{\langle (\Delta\varepsilon_\Delta)^2 \rangle}{\langle \Delta^2 \rangle}}, \tag{12a}$$

$$\varepsilon_{\text{ME}} = \varepsilon_{\text{AUE}} = \frac{1}{\sqrt{N}}\sqrt{\langle \varepsilon_\Delta^2 \rangle}. \tag{12b}$$

Eq. 12a followed the derivation of the root mean square error of prediction in Ref. [47] but remains more conservative by omitting a correction factor of $1/\sqrt{2}$.

2.4 Data sharing

Data related to this work are shared in the GitHub repository *Becksteinlab/SAMPL6_logP_data* that is archived on Zenodo at DOI 10.5281/zenodo.3549988. Input files for Gromacs 2018 and results in CSV format for the SAMPL6 submissions and the improved protocol discussed in Results are included.

3 Results and Discussion

3.1 Validation of octanol parameters

Octanol was parameterized (1) using MOL2FF and the standard OPLS-AA parameters [13] distributed with the GROMACS package, (2) using AmberTools, ACPYPE [25] and GAFF [24] and (3) using the CGenFF server [21, 22] for CHARMM/CGenFF [20]. The parametrization was validated by (1) computing the density as a function of temperature, (2) calculation of the chemical potential, (3) calculation of the hydration free energy, and (4) calculation of the octanol-water partition coefficient and comparison to experimental values.

The bulk density of octanol was calculated from simulations in a 5.6 nm-length cubic box of dry octanol (512 octanol molecules) or wet octanol (374 octanol molecules and 138 water molecules) of 100 ns length at five temperatures from 273 K to 373 K and $P = 1$ bar (Figure 2 and Supplementary Table S1). The experimental data for dry 1-octanol were retrieved from REAXYS (`https://www.reaxys.com`, accessed on 10 September 2019). The simulations of dry and wet octanol with CGenFF, GAFF, and OPLS-AA parameters gave similar results, with the exception of the wet octanol simulation with OPLS-AA parameters at 273 K, as discussed below. The simulated density slightly underestimated the experimental density between -1% at low temperatures and -5.7% near the boiling point of water. The wet octanol density was always higher than the dry octanol density.

The OPLS-AA wet octanol system underwent a phase transition to a dense solid phase during the simulation at 273 K (Figure 2a). The experimental melting temperature of pure octanol is 258.5 K and although water-octanol mixtures will have a different melting temperature, the behavior that we observed here is likely unphysical because similar behavior was recently reported and considered a consequence of exaggerated attractive interactions between the alkane chains of the alcohols in standard OPLS-AA [48]. Because we observed no phase transition in simulations at temperatures around our simulation temperature (300 K) we used the standard OPLS-AA parameters of octanol for the OPLS-AA calculations in this work.

The chemical potential of octanol μ^{octanol} is the transfer free energy of a octanol molecule from vacuum to the pure octanol solvent, $\Delta G_o^{\text{octanol}}$. We calculated $\Delta G_o^{\text{octanol}}$ for all octanol parameters with the FEP protocol described above (Table 1). The hydration free energy of octanol $\Delta G_w^{\text{octanol}}$ was calculated in a similar way and the octanol-water partition coefficient was calculated using Eq. 1. The computed chemical potential values were -7.63 ± 0.16 kcal/mol for GAFF, -8.59 ± 0.16 kcal/mol for OPLS-AA, and -8.98 ± 0.19 kcal/mol for CGenFF, which match the experimen-

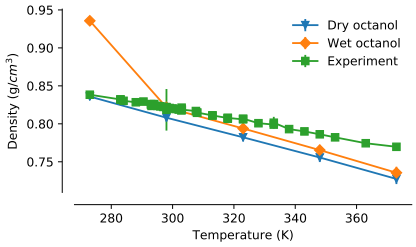

2a **OPLS-AA** octanol parameters and TIP4P water model

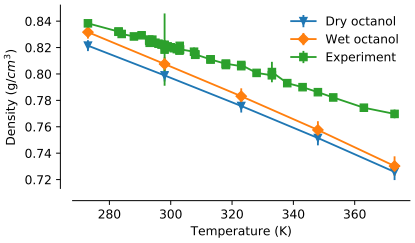

2b **GAFF** octanol parameters and TIP3P water model

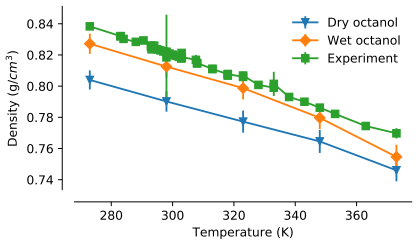

2c **CGenFF** octanol parameters and TIP3P water model

Fig. 2: Dependence of the density of dry and wet octanol on the temperature. Green squares are experimental data; blue triangles were computed from 100-ns MD simulations with dry octanol; orange diamonds were computed from 100-ns MD simulations with wet octanol

tal value -8.13 kcal/mol fairly well. The calculated hydration free energy values of -3.26 ± 0.05 kcal/mol for OPLS-AA and -3.82 ± 0.05 for CGenFF agree fairly well (<1 kcal/mol error) with the experimental value -4.09 ± 0.60 kcal/mol, while the GAFF value -2.62 ± 0.05 kcal/mol was 1.47 kcal/mol higher than the experimental value. The calculated octanol-water partition coefficients for all three octanol models ranged from 3.6 to 3.9 log-units, about 1 log-unit higher than the experimental value 2.92 ± 0.09 kcal/mol.

For GAFF and CGenFF, the parametrization reproduced the density of octanol satisfactorily. For OPLS-AA, we would not recommend using the parameters at lower temperatures but they appear satisfactory at room and higher temperatures. The free energies of solvation matched experimental data reasonably well, with GAFF showing a trend towards undersolvating octanol in both water (like all three force fields) and also in octanol itself. For all three force field parametrizations, the $\log P_{ow}$ is about 1 unit too high, a trend that also became apparent for the SAMPL6 compounds for the OPLS-AA and GAFF force fields, as discussed below.

Table 1: Hydration free energies, chemical potentials and octanol-water partition coefficients for all octanol parameters were calculated and compared with experimental values.

Parametrization	ΔG_w (kcal/mol)	Δ[a]	μ[b] (kcal/mol)	Δ[a]	$\log P_{ow}$	Δ[a]
GAFF	−2.62(5)	1.47(60)	−7.63(16)	0.50(16)	3.65(12)	0.73(15)
OPLS-AA	−3.26(5)	0.83(60)	−8.59(16)	−0.46(16)	3.89(13)	0.97(16)
CGenFF	−3.82(5)	0.27(60)	−8.98(19)	−0.85(19)	3.76(15)	0.84(17)
Exp[c]	−4.09(60)		−8.13		2.92(9)	

[a] The difference Δ (Eq. 8a) between experimental and computed hydration free energies, chemical potentials and octanol-water partition coefficients is shown for each octanol parametrization. The standard error of the mean in the last significant digits is given in parentheses (Eq. 8b).
[b] The chemical potential of octanol μ is the transfer free energy of an octanol molecule from vacuum to the pure octanol solvent ΔG_o.
[c] Experimental $\log P_{ow}$ values were retrieved from REAXYS (`https://www.reaxys.com`). Multiple values were averaged and errors were taken as the standard deviation of the mean. The experimental octanol chemical potential μ (no reported uncertainty) and hydration free energy ΔG_w were retrieved from the Minnesota Solvation Database (`https://comp.chem.umn.edu/mnsol/`); the latter agrees with the value from the FreeSolv database (DOI 10.5281/zenodo.1161245).

3.2 Improvements to the FEP protocol

We started with our standard FEP protocol [6–8], with calculations in the *NPT* ensemble for water, dry octanol, and wet octanol (27 mol % water in octanol) solutions. All $\log P_{ow}$ values were computed from the solvation free energies according to Eq. 1. After submission and release of the experimental values, we made two changes to our protocol, which are discussed in more detail below: We switched our estimators to use our new ALCHEMLYB library [35] and we added an equilibration phase to the FEP windows by discarding the first nanosecond during preprocessing (also made easy by the preprocessing module in ALCHEMLYB).

3.2.1 Estimator comparison

The $\log P_{ow}$ results submitted to the SAMPL6-logP challenge as entries **cp8kv**, **623c0** (OPLS-AA (mol2ff) dry/wet), **eufcy**, **mwuua** (OPLS-AA (LigParGen) dry/wet), **sqosi**, **6nmtt** (GAFF dry/wet), and **3oqhx** (CGenFF dry) (Supplementary Tables S4–S7 in the Supplementary Information) were calculated with the MDPOW-TI estimator, which uses all data but decorrelates the data for the error estimation [6]. We have been developing the ALCHEMLYB library [35] as a reference FEP analysis library to be used as a drop-in replacement for in-house code. We took the analysis of the SAMPL6 data as an opportunity to switch MDPOW to using ALCHEMLYB and in particular, to use alchemlyb's MBAR estimator. We first established that MDPOW-TI (Simpson's rule) and ALCHEMLYB-TI (trapezoid rule) gave similar results when applied to all data, with typical root mean square differences (RMSD) close to 0 (range 0.10–0.15; see Supplementary Figure S1). Furthermore, ALCHEMLYB-MBAR also gave similar $\log P_{ow}$-values as the two TI estimates (RMSDs 0.04–0.21). The estimated uncertainties from ALCHEMLYB were, however, much smaller than the ones from MDPOW because the raw data were highly correlated. To estimate the uncer-

Table 2: *RMSE*, *AUE* and *ME* when all data in each λ window (0–5 ns) was used and when the first nanosecond was discarded as equilibration (1–5 ns).

parameter	oct	all (0–5 ns)			equilibrated (1–5 ns)			Entry[a]
		RMSE	AUE	ME	RMSE	AUE	ME	
OPLS-AA	dry	2.83(5)	2.68(5)	2.68(5)	2.79(5)	2.61(5)	2.61(5)	**cp8kv**
OPLS-AA	wet	2.62(5)	2.50(4)	2.50(4)	2.72(5)	2.61(5)	2.61(5)	**623c0**
LigParGen	dry	1.90(6)	1.79(6)	1.66(6)	1.71(6)	1.57(6)	1.57(6)	**eufcy**
LigParGen	wet	1.80(6)	1.68(6)	1.68(6)	1.62(6)	1.51(6)	1.51(6)	**mwuua**
GAFF	dry	2.36(8)	2.13(7)	2.13(7)	1.52(7)	1.28(7)	1.28(7)	**sqosi**
GAFF	wet	2.26(7)	2.07(7)	2.07(7)	1.71(8)	1.48(7)	1.48(7)	**6nmtt**
CGenFF	dry	1.08(6)	0.90(6)	0.24(6)	1.17(5)	0.91(6)	−0.32(6)	**3oqhx**
CGenFF	wet	1.48(5)	1.21(5)	0.16(5)	1.42(5)	1.05(5)	−0.10(5)	—[b]

[a] The corresponding submission entry codes for the raw data used to calculate the results. Entries in this table were processed with ALCHEMLYB-MBAR and are not the results that were submitted to SAMPL6; instead see Tables S4–S7 in the Supplementary Information for the submitted results, which were processed with MDPOW-TI (Simpson's rule). [b] Results with CGenFF in wet octanol had not been submitted to SAMPL6 but were computed for this work to enable a complete comparison.

tainties free of bias, uncorrelated data were generated by applying the autocorrelation analysis to simulations for all λ windows, according to Eqs. 2–4; the resulting ALCHEMLYB uncertainties were comparable to the ones obtained with the MDPOW-TI estimator.

This preliminary analysis established that we could safely replace the MDPOW-TI estimator with the ALCHEMLYB ones. Given that ALCHEMLYB-TI and MBAR gave similar answers (RMSDs 0.04–0.10) we focused on results with the MBAR estimator which, at least in principle, makes better use of the available data [34].

3.2.2 The importance of equilibration

In our simulation protocol we used all data from each FEP window because in previous SAMPL challenges with water and cyclohexane we were concerned with sufficient sampling and had no indication that windows might require appreciable equilibration time. However, David Mobley's group shared with us their AMBER/GAFF results, which were more accurate than our AMBER/GAFF results (their RMSE 1.6 compared to our 2.4, Table 2) even though the force field and overall protocol seemed similar [49]. The root mean square difference (RMSD) between the two data sets for dry octanol was 2.3 (our **sqosi** *vs* **REF07** from Ref. [49]) with a similar RMSD of 2.4 for wet octanol (**6nmtt** *vs* **REF02**) as shown in Figure S5 in the Supplementary Information. (Işık *et al* [49] discussed a comparison between the different simulations in more detail and concluded that octanol equilibration period, assignment of charges to carboxylic acids, and also tautomer selection all contributed to different results.)

One major difference between the protocols appeared to be that the Mobley group followed their own best practices and eliminated any non-equilibrated region of the trajectories [43], which was particularly important for the octanol simulations [49]. We therefore discarded the first 1 ns of all trajectories as equilibration and re-computed all free energies and $\log P_{ow}$ from the data at 1–5 ns in each FEP window. Comparing

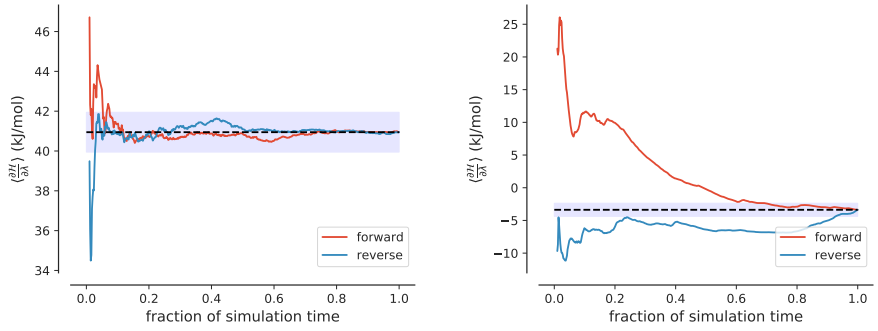

3a water, $\lambda_{Coul} = 1$ and $\lambda_{vdW} = 0.3$

3b wet octanol, $\lambda_{Coul} = 0.375$ and $\lambda_{vdW} = 0$

Fig. 3: $\left\langle \frac{\partial \mathscr{H}}{\partial \lambda} \right\rangle$ time-reversed and time-forward convergence plots for **SM14**. 3a The calculated convergence time fraction R_c was 0.05, indicating a well equilibrated window. 3b The calculated R_c was 0.89, indicating that this window was not well equilibrated.

the RMSE for using all data (0–5 ns) with the equilibrated (1–5 ns) values showed that leaving out the first nanosecond lead to a large improvement for the GAFF results, which decreased by 0.84 log units to 1.53 for dry octanol and by 0.55 log units to 1.71 for wet octanol (Table 2). The improvement for OPLS-AA (LigParGen) was modest (decreased by 0.19 and 0.18), about within uncertainties for OPLS-AA (mol2ff) and CGenFF, where it marginally worsened the RMSE by 0.09.

Because of the large improvement in the RMSE for the GAFF simulations we sought to assess equilibration behavior. As an example we investigated **SM14** for which omitting the equilibration improved agreement with experiment by about 1.5 log units. Time-reversed convergence plots [43, 50] were used to determine the non-equilibrated region in each λ window. We calculated the time-forward average and time-reversed average of $\frac{\partial \mathscr{H}}{\partial \lambda}$ by

$$\left\langle \frac{\partial \mathscr{H}}{\partial \lambda} \right\rangle_t = \frac{t}{T} \sum_{t'=0}^{t} \left. \frac{\partial \mathscr{H}}{\partial \lambda} \right|_{t'} \tag{13}$$

$$\left\langle \frac{\partial \mathscr{H}}{\partial \lambda} \right\rangle_{-t} = \frac{t}{T} \sum_{t'=T-t}^{T} \left. \frac{\partial \mathscr{H}}{\partial \lambda} \right|_{t'} \tag{14}$$

For a simulation with a time length of T, the convergence time t_c was defined as the smallest time t for which both the forward and the reverse average were within $\varepsilon = 1$ kJ/mol of the value computed over all T,

$$t_c = \arg\min_t \left(\left| \left\langle \frac{\partial \mathscr{H}}{\partial \lambda} \right\rangle_t - \left\langle \frac{\partial \mathscr{H}}{\partial \lambda} \right\rangle_T \right| < \varepsilon \wedge \left| \left\langle \frac{\partial \mathscr{H}}{\partial \lambda} \right\rangle_{-t} - \left\langle \frac{\partial \mathscr{H}}{\partial \lambda} \right\rangle_T \right| < \varepsilon \right). \tag{15}$$

For example, Figure 3a shows an example where the forward and reverse averages rapidly approach the ε band around the final average, which is indicative of rapid

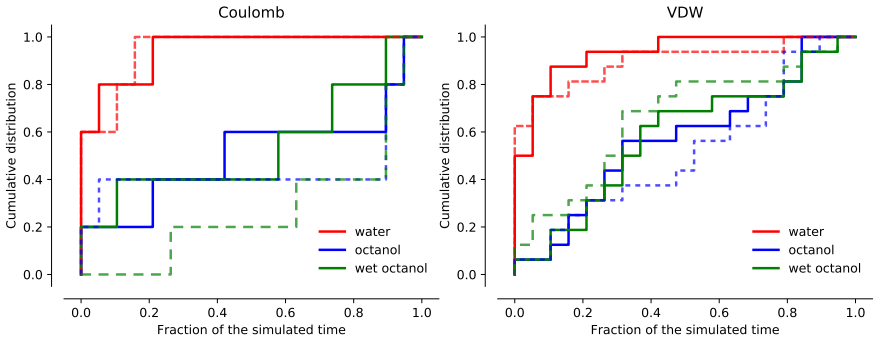

Fig. 4: Cumulative distribution functions $\mathscr{C}(R_c)$ of the convergence time fraction R_c for Coulomb and VDW λ windows from all data (0–5 ns) (dashed lines) and data with the first 1 ns discarded as equilibration (1–5 ns) (solid lines) for **SM14** (GAFF).

equilibration. On the other hand, Figure 3b shows an example that is poorly equilibrated because forward and reverse averages only come close near the very end of the simulation time.

To make the time point of convergence easily comparable, we defined the convergence time fraction R_c as

$$R_c = \frac{t_c}{T}. \tag{16}$$

R_c denotes the fraction of the simulation time from which on the system appears to be equilibrated, with $R_c = 0$ indicating the system is well equilibrated at the beginning, and $R_c = 1$ that the whole trajectory is not equilibrated.

Using R_c as a measure of convergence, we analyzed the complete set of λ windows for **SM14** by computing $R_c(\lambda)$ for each window and then plotting a cumulative probability distribution function $\mathscr{C}(R_c) = \mathscr{P}\big(R_c(\lambda) \leq R_c\big)$ of these values, which measures what fraction of windows has at least the given R_c. For a perfectly equilibrated FEP calculation, $\mathscr{C}(R_c)$ resembles a unit step function near $R_c = 0$ because all windows have $R_c(\lambda) \approx 0$. For a poorly equilibrated calculation, $\mathscr{C}(R_c)$ rises steeply near $R_c = 1$.

The cumulative distributions of the convergence time fractions, $\mathscr{C}(R_c)$, of all Coulomb and VDW windows from the whole data (all data, 0–5 ns) for **SM14** and GAFF showed that the water simulations equilibrated much faster than the dry and the wet octanol simulations (Figure 4). This behavior was particularly apparent for the Coulomb part of the calculation. The data discarding the first 1 ns (reduced data, 1–5 ns) showed the same trends, with water simulations reaching equilibrium after about 20% of the simulation time (Figure 4). Discarding the first 1 ns as equilibration improved the equilibration behavior of the Coulomb part of the octanol simulations as shown by the "1–5 ns" $\mathscr{C}(R_c)$ graph (solid line) emerging above the "0–5 ns" graph in Figure 4. Despite this improvement, overall convergence of the octanol simulation windows remained poor.

Table 3: Equilibration ratio A_c of all data (0–5 ns) and reduced data (1–5 ns) for **SM14** (GAFF), separated by FEP Coulomb and VDW windows.

	Water		*Dry* Octanol		*Wet* Octanol	
	Coulomb	VDW	Coulomb	VDW	Coulomb	VDW
0–5 ns	0.95	0.90	0.44	0.51	0.27	0.66
1–5 ns	0.95	0.93	0.51	0.57	0.54	0.58

Instead of using visual comparison of $\mathscr{C}(R_c)$ graphs, we sought to define a quantitative quality measure for the convergence of a whole set of λ windows in the form of a single number. The area A_c under the cumulative distribution $\mathscr{C}(R_c)$,

$$A_c = \int_0^1 \mathscr{C}(R_c)\, dR_c, \tag{17}$$

turned out to be a suitable quantity with a simple interpretation. A_c is a number between 0 and 1 because it is based on a cumulative probability function (monotonically increasing from 0 to 1) that is integrated over the range 0 to 1. A_c can be interpreted as the ratio of the equilibrated simulation time to the whole simulation time for a set of simulations. $A_c = 1$ means that all simulation time frames in all windows can be considered equilibrated (with the meaning of Eq. 15), while $A_c = 0$ indicates that nothing is equilibrated.

For example, the equilibration ratios A_c of all Coulomb and VDW windows from both all data and reduced data for **SM14** (Table 3) showed that over 90% of the sampled time of water simulations was equilibrated. One the other hand, the dry and the wet octanol simulations only had A_c ranging from 0.27 to 0.66, again indicating poorly equilibrated octanol simulations.

Although dry octanol and wet octanol results indicated a lack of equilibration in both data sets for **SM14**, discarding the first nanosecond improved the convergence behavior of the Coulomb part. Specifically, A_c for the Coulomb windows in dry octanol improved from 0.44 to 0.51 and from 0.27 to 0.54 for wet octanol (Table 3). For the wet octanol VDW simulations, discarding data slightly worsened equilibration as seen in the equilibration ratio decrease from 0.66 to 0.68. Nevertheless, for all other windows, discarding the initial part of the windows improved A_c (Table 3).

To test whether A_c could describe the equilibration of the simulations, we ran longer FEP simulations for **SM14** (GAFF) using a protocol with one initial 100 ns NPT equilibrium simulation and 50 ns production simulations for each window. As expected, the ten-fold longer simulation time improved convergence in all cases, with the largest increase in A_c for the wet octanol Coulomb windows from 0.27 to 0.69 (Figure S4 and Table S3 in the Supplementary Information).

The picture across the whole data set of GAFF simulations was not as striking as for **SM14** although discarding the first nanosecond also improved A_c for the octanol simulations from 0.44 to 0.46 (dry) and 0.40 to 0.47 (wet), as shown in Table S2 and Figure S3 in the Supplementary Information. For almost all force fields, the reduced data showed better equilibration ratios than the 0–5 ns data, with the occasional small

decrease by up to 0.02. The OPLS-AA (LigParGen) simulations were the only ones with exceptional behavior in that the reduced simulations had a markedly decreased water Coulomb A_c from 0.85 to 0.76 but a substantially increased octanol Coulomb A_c from 0.27 to 0.49 (dry) and 0.35 to 0.42 (wet).

These data suggested an overall improvement in convergence due to discarding an initial equilibration phase in each λ-window, so we decided to take equilibration into account, in line with FEP best practices [43]. For simplicity, we applied the 1 ns equilibration time to all data sets; in the future, this could certainly be optimized for individual data sets, using, for instance A_c (Eq. 17). (We also attempted to use the *equilibrium detection algorithm* [44] as implemented in alchemlyb's `preprocessing.subsampling.equilibrium_detection()` function but did not manage to obtain consistent and robust results for the equilibration period.)

3.3 Predicted partition coefficients

For all eleven molecules (Figure 1), absolute solvation free energy calculations were carried out using topologies generated with standard OPLS-AA atom types with fixed charges (referred to as *OPLS-AA (mol2ff)* or simply *OPLS-AA*), OPLS-AA with variable 1.14*CM1A charges (*OPLS-AA (LigParGen)* or just *LigParGen*), and AMBER/GAFF (*GAFF*). CHARMM/CGenFF (*CGenFF*) topologies for eight of the eleven molecules were used to calculate solvation free energies; three halogen-containing molecules were omitted as explained in Methods (Section 2.1). We included the CGenFF results for the eight compounds because when we calculated the RMSE for the other three force fields for the same eight compounds as for CGenFF (Supplementary Table S8), the difference compared to calculating it over all eleven values (Table 2) was small.

As the effect of equilibration was sizable and the preliminary analysis in terms of A_c (Eq. 17) indicated systematic improvements, we decided to treat the first 1 ns as equilibration for all data sets. Thus, the following detailed results for $\log P_{ow}$ differ from the submitted results in that (1) a 1 ns equilibration time was discarded for each FEP window and (2) the free energies were calculated with the MBAR estimator.

The predictions were compared to the experimental values, with a summary for all eight data sets shown in Table 2. In addition to RMSE, AUE, and ME, the Pearson correlation coefficient and the Kendall rank correlation coefficients were calculated, although the sample size might not be big enough to adequately capture the statistics. In the following we discuss in more detail the individual data sets, sorted by force field parametrization.

*3.3.1 OPLS-AA (*MOL2FF*)*

OPLS-AA with transferable charges did not perform well. The RMSE was 2.79 ± 0.05 for dry octanol and 2.72 ± 0.05 for wet octanol (Table 4). The correlation between experimental and computed values in Figure 5 showed none of the compounds were within one log unit, most were off by 2 to 3 log units, with **SM08** off by 5 log units. The Pearson correlation coefficients *r* for the dry and the wet calculations were

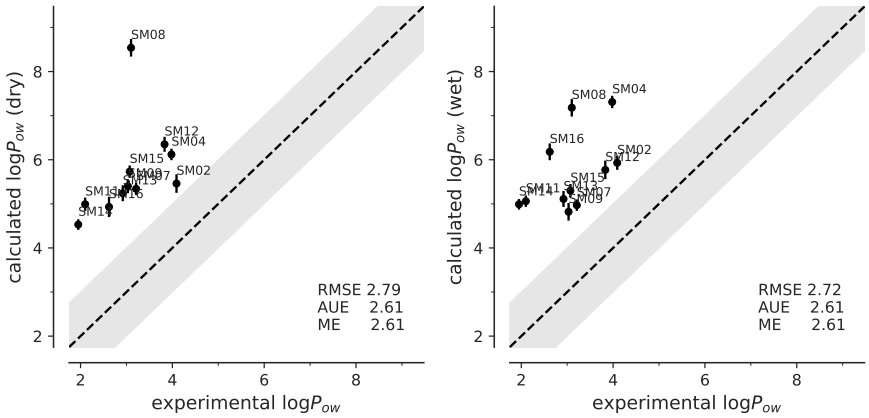

Fig. 5: Correlation between experimental and computed octanol-water coefficients $\log P_{ow}$ for simulations performed with dry or wet octanol with OPLS-AA (mol2ff) parameters. The gray band indicates ± 1 log-units from ideal correlation, shown by the dashed line. The root mean square error (RMSE), the absolute unsigned error (AUE), and the (signed) mean error (ME) are indicated. Error bars represent the error in the experiments or the error on the mean, derived from the simulations.

0.41 and 0.49 (with $r = 1$ indicating perfect correlation, 0 no correlation, and -1 perfect anticorrelation), summarizing the moderate success in quantitatively predicting $\log P_{ow}$. The Kendall rank correlation coefficient τ was computed to evaluate the ability to rank-order the data; a value of $\tau = 1$ indicates that the simulations predict the same ranking of compounds by $\log P_{ow}$ as the experimental data whereas if the rankings were completely reversed τ would obtain the value -1 and if the simulations produced random results, a value close to 0 would be expected. The dry octanol data yielded $\tau = 0.60$, better than the value of 0.38 for the wet octanol predictions. The dry octanol simulations were moderately successful at rank-ordering compounds, while the wet octanol ones did not perform well.

The AUE (2.61) was the same as the absolute value of ME for both the dry and wet octanol, which corresponds to the visual inspection of the correlation plot (Figure 5) that all the prediction were larger than the experimental values. If we corrected our results by shifting the values by the ME, then the shifted dry octanol data would have had an RMSE of 0.97 instead of 2.79; the shifted wet octanol data would have had an RMSE of 0.78 instead of 2.72, which would have constituted a dramatic improvement.

Overall, these results suggested a systematic error in OPLS-AA calculations that overestimated the $\log P_{ow}$. As in our previous work on cyclohexane distribution coefficients [8] (and unpublished data) we suspect that the primary problem lies with the hydration free energy calculations, which are too positive, i.e., the molecules are under-solvated in water.

Table 4: Computed ($\log P_{ow}$) and experimental ($\log P_{ow}^{\mathrm{exp}}$) octanol-water partition coefficients with error estimate for the **OPLS-AA (mol2ff)** results processed with ALCHEMLYB-MBAR. The same raw data processed with MDPOW-TI (Simpson's rule) were submitted as entries **cp8kv** (Protocol *Dry*) and **623c0** (Protocol *Wet*), see Table S4 in the Supplementary Information

id	Exp.	*Dry* Octanol		*Wet* Octanol	
	$\log P_{ow}^{\mathrm{exp}}$	$\log P_{ow}$	Δ[a]	$\log P_{ow}$	Δ[a]
SM02	4.09(3)	5.46(21)	1.37(21)	5.93(16)	1.84(16)
SM04	3.98(3)	6.12(13)	2.14(13)	7.31(14)	3.33(14)
SM07	3.21(4)	5.34(14)	2.13(14)	4.97(13)	1.76(13)
SM08	3.1(3)	8.54(20)	5.44(20)	7.18(20)	4.08(20)
SM09	3.03(7)	5.4(16)	2.37(17)	4.82(20)	1.79(21)
SM11	2.1(4)	4.99(15)	2.89(15)	5.06(13)	2.96(13)
SM12	3.83(3)	6.35(17)	2.52(17)	5.77(21)	1.94(21)
SM13	2.92(4)	5.24(18)	2.32(18)	5.11(18)	2.19(18)
SM14	1.95(3)	4.53(12)	2.58(12)	4.99(12)	3.04(12)
SM15	3.07(3)	5.73(14)	2.66(14)	5.3(15)	2.23(15)
SM16	2.62(1)	4.93(23)	2.31(23)	6.18(19)	3.56(19)
RMS Error (RMSE)[b]			2.79(5)		2.72(5)
Absolute Unsigned Error (AUE)			2.61(5)		2.61(5)
Mean Error (ME)			2.61(5)		2.61(5)

[a] The difference Δ (Eq. 8a) between experimental and computed octanol-water partition coefficients is shown for each compound. The standard error of the mean in the last significant digits is given in parentheses (Eq. 8b).
[b] The root mean square error (RMSE), the absolute unsigned error (AUE), and the signed mean error (ME) were calculated according to Eqs. 9–11.

3.3.2 OPLS-AA (LigParGen)

OPLS-AA with non-transferable charges performed somewhat better than OPLS-AA with transferable charges, although the same tendencies remained: The RMSE was 1.71 ± 0.07 for the dry octanol and 1.62 ± 0.07 for wet octanol (Table 5). An improvement of about 0.2 log units in RMSE was obtained by removing the equilibrium part. While a few compounds such as **SM14** and **SM15** were within one log unit, most were off by 1 to 2.5 log units (Figure 6). The Pearson correlation coefficients r for the dry and the wet calculations were 0.78 and 0.60, summarizing the moderate success in quantitatively predicting $\log P_{ow}$. The dry octanol data yielded the Kendall rank correlation coefficient $\tau = 0.64$, slightly better than the value of 0.56 for the wet octanol predictions. Both the dry and wet octanol simulations were moderately successful at rank-ordering compounds.

Similar to the OPLS-AA (mol2ff) results, the AUE (1.57 for dry and 1.51 for wet) was the same as the absolute value of ME for both the dry and wet octanol, which again indicated a systematical shift in the calculated results. Shifting the values by the ME would have improved the dry octanol RMSE to 0.68 instead of 1.71

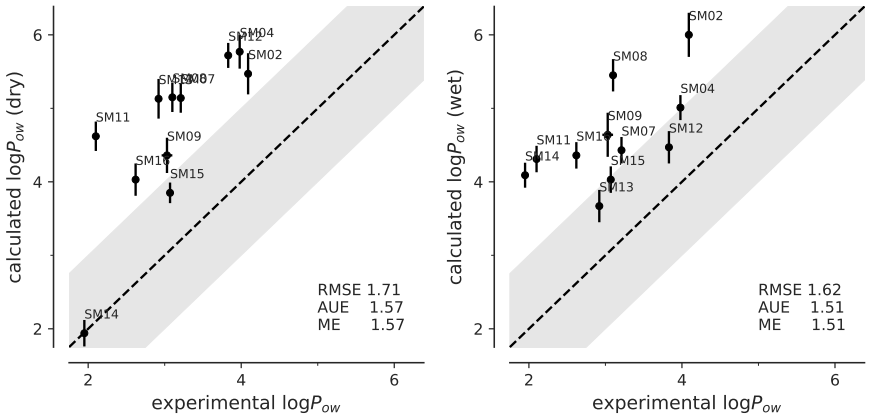

Fig. 6: Correlation between experimental and computed octanol-water coefficients $\log P_{ow}$ for simulations performed with dry or wet octanol with OPLS-AA (LigParGen) parameters.

and wet octanol RMSE to 0.59 instead of 1.61, which would have been a 1-log-unit improvement.

Compared to OPLS-AA with transferable charges, OPLS-AA with non-transferable CM1A charges produced a better prediction but still suffered from a large systematic error, likely related to hydration. It appears that sacrificing the transferability of the original OPLS-AA atom types can buy moderately higher accuracy at the cost of having to parameterize the charges for every single molecule.

3.3.3 GAFF

As mentioned before, the GAFF parametrization benefited most from implementing the equilibration preprocessing, which turned the poor initial GAFF accuracy into a reasonably good one, by lowering the RMSE by 0.84 log units. The RMSE was 1.52 ± 0.08 for the dry octanol and 1.71 ± 0.08 for wet octanol (0.55 lower) (Table 6). In Figure 7, several compounds like **SM11**, **SM14** and **SM15** were within one log unit, most of the other compounds were off by 1 to 2 log units, with **SM13** as far as 3.6. The Pearson correlation coefficients r for the dry and the wet calculations were 0.80 and 0.71, showing a better ability to quantitatively predict $\log P_{ow}$. The Kendall rank correlation coefficient for the dry octanol simulations was 0.53, slightly worse than the wet octanol predictions with $\tau = 0.59$. Both the dry and wet octanol simulations were moderately successful at rank-ordering compounds.

Similar to both OPLS-AA results, the AUE (1.28 for dry and 1.48 for wet) was the same as the absolute value of ME for both the dry and wet octanol, which also indicated a systematical error in the calculated results. After subtracting the ME from the results, the dry octanol data would have had an RMSE of 0.83 instead of 1.52;

Table 5: Computed ($\log P_{ow}$) and experimental ($\log P_{ow}^{\mathrm{exp}}$) octanol-water partition coefficients with error estimate for the **OPLS-AA (LigParGen)** results processed with ALCHEMLYB-MBAR. The same raw data processed with MDPOW-TI (Simpson's rule) were submitted as entries **eufcy** (Protocol *Dry*) and **mwuua** (Protocol *Wet*), see Table S5 in the Supplementary Information

id	Exp.	*Dry* Octanol		*Wet* Octanol	
	$\log P_{ow}^{\mathrm{exp}}$	$\log P_{ow}$	Δ	$\log P_{ow}$	Δ
SM02	4.09(3)	5.47(28)	1.38(28)	6.0(30)	1.91(30)
SM04	3.98(3)	5.77(23)	1.79(23)	5.01(17)	1.03(17)
SM07	3.21(4)	5.14(20)	1.93(20)	4.43(18)	1.22(18)
SM08	3.1(3)	5.15(20)	2.05(20)	5.45(22)	2.35(22)
SM09	3.03(7)	4.36(24)	1.33(25)	4.64(30)	1.61(30)
SM11	2.1(4)	4.62(20)	2.52(20)	4.31(18)	2.21(18)
SM12	3.83(3)	5.72(17)	1.89(17)	4.47(22)	0.64(22)
SM13	2.92(4)	5.13(27)	2.21(27)	3.67(22)	0.75(22)
SM14	1.95(3)	1.94(18)	−0.01(18)	4.09(17)	2.14(17)
SM15	3.07(3)	3.85(14)	0.78(14)	4.03(18)	0.96(18)
SM16	2.62(1)	4.03(22)	1.41(22)	4.36(18)	1.74(18)
RMS Error (RMSE)			1.71(7)		1.62(7)
Absolute Unsigned Error (AUE)			1.57(7)		1.51(7)
Mean Error (ME)			1.57(7)		1.51(7)

the wet octanol data would have had an RMSE of 0.86 instead of 1.71, resulting in a 0.8-log-unit improvement.

Our calculations showed a systematic error in our GAFF calculations but it is not clear that it has the same basis as the one for OPLS-AA. For OPLS-AA we can draw on other data for the hypothesis that water-solute interactions might be at the core of the problem. For GAFF we do not have the same data available but future analysis of our data in the context of other SAMPL6-logP submissions might indicate problematic areas. Nevertheless, the overall performance of GAFF, especially after equilibration, was reasonably good.

3.3.4 CGenFF

The compounds **SM04**, **SM12** and **SM16** contained halogens with lone pairs and could therefore not be processed with the `cgenff_charmm2gmx.py` script so that we were not able to obtain Gromacs CGenFF parameters (see Section 2.1). Hence we excluded these three compounds and only report results for the remaining eight compounds.

The CGenFF results were qualitatively different from the OPLS-AA and AMBER/GAFF results in almost all aspects: The RMSE was 1.17 ± 0.06 for the dry octanol and 1.42 ± 0.06 for wet octanol (Table 7), and removing the equilibration period showed no improvement. This behavior could indicate that the CGenFF simulations equilibrated faster or that the set-up protocol prepared them in a state closer resembling equilibrium. Either way, one of our lessons of this study is that careful analysis

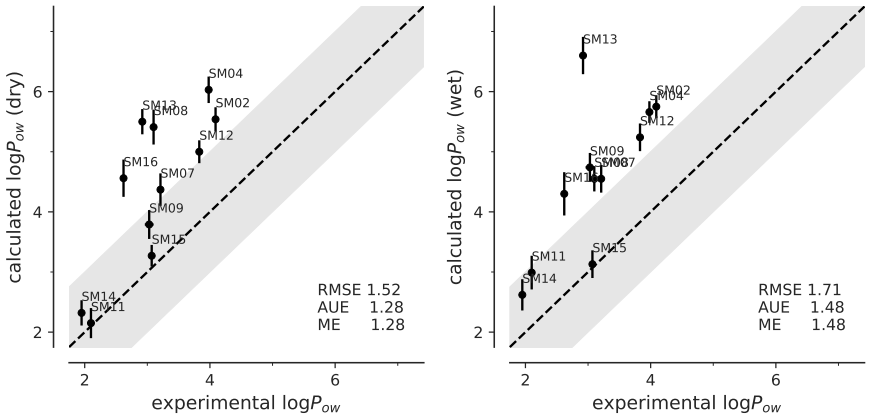

Fig. 7: Correlation between experimental and computed octanol-water coefficients $\log P_{ow}$ for simulations performed with dry or wet octanol with GAFF parameters.

Table 6: Computed ($\log P_{ow}$) and experimental ($\log P_{ow}^{\mathrm{exp}}$) octanol-water partition coefficients with error estimate for the **GAFF** results processed with ALCHEMLYB-MBAR. The same raw data processed with MDPOW-TI (Simpson's rule) were submitted as entries **sqosi** (Protocol *Dry*) and **6nmtt** (Protocol *Wet*), see Table S6 in the Supplementary Information

id	Exp.	*Dry* Octanol		*Wet* Octanol	
	$\log P_{ow}^{\mathrm{exp}}$	$\log P_{ow}$	Δ	$\log P_{ow}$	Δ
SM02	4.09(3)	5.54(20)	1.45(20)	5.75(19)	1.66(19)
SM04	3.98(3)	6.03(22)	2.05(22)	5.66(18)	1.68(18)
SM07	3.21(4)	4.37(27)	1.16(27)	4.55(23)	1.34(23)
SM08	3.1(3)	5.41(28)	2.31(29)	4.55(21)	1.45(21)
SM09	3.03(7)	3.79(24)	0.76(25)	4.74(24)	1.71(25)
SM11	2.1(4)	2.15(25)	0.05(25)	2.99(28)	0.89(28)
SM12	3.83(3)	5.0(19)	1.17(19)	5.24(23)	1.41(23)
SM13	2.92(4)	5.5(21)	2.58(21)	6.6(31)	3.68(31)
SM14	1.95(3)	2.32(21)	0.37(21)	2.62(26)	0.67(26)
SM15	3.07(3)	3.27(18)	0.20(18)	3.13(23)	0.06(23)
SM16	2.62(1)	4.56(31)	1.94(31)	4.3(36)	1.68(36)
RMS Error (RMSE)			1.52(8)		1.71(8)
Absolute Unsigned Error (AUE)			1.28(7)		1.48(8)
Mean Error (ME)			1.28(7)		1.48(8)

of convergence should be carried out regardless of the force field. In Figure 8, about half of the compounds were within one log unit, with the others off by 1 to 2.5. The Pearson correlation coefficients r for the dry and the wet calculations were 0.27 and 0.16. The dry octanol data yielded a Kendall rank correlation coefficient $\tau = 0.29$, and the value for the wet octanol predictions was 0.07. These coefficients indicated a

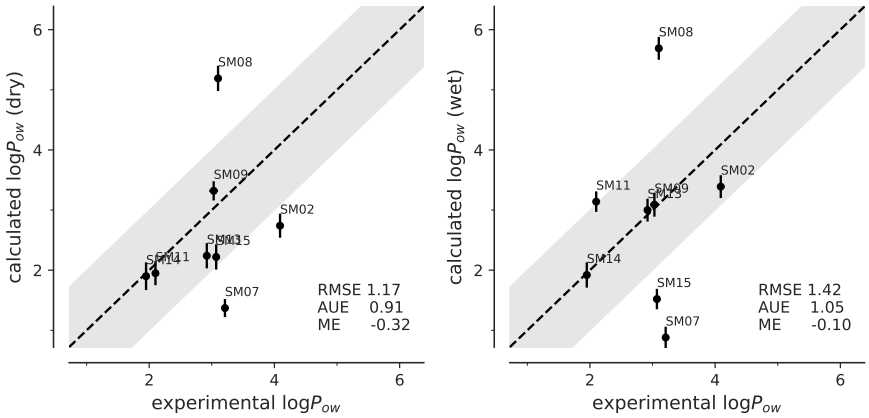

Fig. 8: Correlation between experimental and computed octanol-water coefficients $\log P_{ow}$ for simulations performed with dry or wet octanol with CGenFF parameters.

poor ability rank-ordering the data although eight samples might not be enough to obtain reasonable results from these correlation analysis tools. Different from previous results, no systematic shift in the CGenFF results was observed from the AUE (0.91 for dry and 1.05 for wet) and the absolute value of ME (-0.32 for dry and -0.10 for wet).

In terms of RMSE, the CGenFF parametrization produced the best result. This remained true when the RMSEs for the other three parametrizations were also only calculated for the eight compounds for which CGenFF data were available (Supplementary Table S8). However, eight data points might not be enough to properly assess the true accuracy, as indicated by the poor Pearson and Kendall coefficients.

It is encouraging that CGenFF did not exhibit an obvious systematic shift, which suggested that the observed shift for OPLS-AA and GAFF was not an inherent problem in our FEP protocol but was more closely tied to the specific force field implementation (including the water model). The use of different water models in simulations with OPLS-AA (TIP4P) on the one hand, and GAFF or CGenFF (TIP3P) on the other, could contribute to the differences that we observed in our predictions. As noted previously [51, 52], TIP3P has a lower dielectric constant than TIP4P and this could give rise to lower hydration free energies compared to TIP4P. More generally, the OPLS-AA and AMBER/GAFF (and to some degree CHARMM/CGenFF) force fields are known to be underpolarized [53, 54], which also leads to systematically too positive hydration free energies for small molecules [54].

3.4 Effect of tautomers

For **SM08** we originally chose and submitted **micro010** (**SM08_10**), based on the assumption that the aromaticity of the pyridine ring with the potential hydrogen bond of the hydroxyl with the carboxylate would make it the most stable one. However,

Table 7: Computed ($\log P_{ow}$) and experimental ($\log P_{ow}^{\mathrm{exp}}$) octanol-water partition coefficients with error estimate for the **CGenFF** results processed with ALCHEMLYB-MBAR. The same raw data processed with MDPOW-TI (Simpson's rule) were submitted as entry **3oqhx** for Protocol *Dry* (protocol *Wet* was not submitted), see Table S7 in the Supplementary Information

id	Exp.	*Dry* Octanol		*Wet* Octanol	
	$\log P_{ow}^{\mathrm{exp}}$	$\log P_{ow}$	Δ	$\log P_{ow}$	Δ
SM02	4.09(3)	2.74(20)	−1.35(20)	3.39(19)	−0.70(19)
SM07	3.21(4)	1.37(15)	−1.84(15)	0.88(18)	−2.33(18)
SM08	3.1(3)	5.19(21)	2.09(21)	5.69(19)	2.59(19)
SM09	3.03(7)	3.32(16)	0.29(17)	3.09(20)	0.06(21)
SM11	2.1(4)	1.95(20)	−0.15(20)	3.14(17)	1.04(17)
SM13	2.92(4)	2.24(21)	−0.68(21)	3.0(19)	0.08(19)
SM14	1.95(3)	1.9(23)	−0.05(23)	1.92(21)	−0.03(21)
SM15	3.07(3)	2.22(21)	−0.85(21)	1.52(17)	−1.55(17)
RMS Error (RMSE)			1.17(6)		1.42(6)
Absolute Unsigned Error (AUE)			0.91(6)		1.05(6)
Mean Error (ME)			−0.32(6)		−0.10(6)

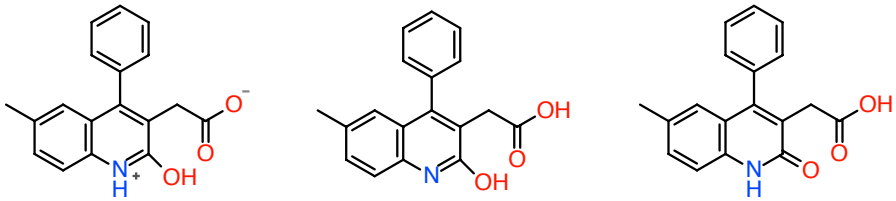

SM08 micro008 **SM08 micro010** **SM08 micro011**

Fig. 9: Chemical structures of the three microstates of compound **SM08** evaluated in this study.

contrary to our chemical intuition, the ground state energies from quantum chemical optimization calculations with the CPCM continuous water model [9] showed that **micro011** (Figure 9) seemed to be the most stable (about 6 kcal/mol lower than **micro010**). In the same conditions, the zwitterionic **micro008** (Figure 9) was about 3.5 kcal/mol more stable than **micro010**. We therefore also computed the octanol-water coefficients for **micro008** (**SM08_08**) and **micro011** (**SM08_11**) (Figure 9). The results in Table 8 indicated that **micro011** gave closer predictions to the experimental values for both dry and wet octanol with the four parametrization methods with a 0.2 to 1 log unit improvement in the RMSE, while were unable to reproduce the experimental values with **micro008**.

These tautomer calculations indicated that the choice of tautomer could have a large effect on calculated $\log P_{ow}$ values. However, from this single example it was

Table 8: Computed ($\log P_{ow}$) and experimental ($\log P_{ow}^{\mathrm{exp}}$) octanol-water partition coefficients with error estimate for the three microstates of compound **SM08**.

id	Exp.	*Dry* Octanol		*Wet* Octanol		Parametrization
	$\log P_{ow}^{\mathrm{exp}}$	$\log P_{ow}$	Δ	$\log P_{ow}$	Δ	
SM08_08	3.1(3)	−1.8(83)	−4.90(83)	1.0(56)	−2.10(56)	OPLS-AA
SM08_08	3.1(3)	1.05(39)	−2.05(39)	3.2(43)	0.10(43)	LigParGen
SM08_08	3.1(3)	4.31(44)	1.21(44)	4.64(32)	1.54(32)	GAFF
SM08_08	3.1(3)	−0.78(85)	−3.88(85)	1.6(43)	−1.50(43)	CGenFF
SM08_10	3.1(3)	8.54(20)	5.44(20)	7.18(20)	4.08(20)	OPLS-AA
SM08_10	3.1(3)	5.15(20)	2.05(20)	5.45(22)	2.35(22)	LigParGen
SM08_10	3.1(3)	5.41(28)	2.31(29)	4.55(21)	1.45(21)	GAFF
SM08_10	3.1(3)	5.19(21)	2.09(21)	5.69(19)	2.59(19)	CGenFF
SM08_11	3.1(3)	6.58(21)	3.48(21)	6.55(23)	3.45(23)	OPLS-AA
SM08_11	3.1(3)	4.03(24)	0.93(24)	4.48(28)	1.38(29)	LigParGen
SM08_11	3.1(3)	3.53(39)	0.43(39)	5.01(17)	1.91(17)	GAFF
SM08_11	3.1(3)	4.11(33)	1.01(33)	5.59(21)	2.49(21)	CGenFF

not clear that the quantum chemical calculations in implicit solvent provided the correct free energy differences between tautomers that would allow one to calculate the proper statistical mechanical average over all tautomer free energies [9]. Clearly, more work is needed to establish a consistent protocol that takes all important tautomers into consideration.

4 Conclusions

We used explicit solvent all-atom MD simulations using four different force field parametrizations (standard OPLS-AA with transferable charges, OPLS-AA with non-transferable CM1A charges, AMBER/GAFF, and CHARMM/CGenFF) to predict water-octanol partition coefficients for the eleven compounds included in the SAMPL6-logP challenge. Force field parameters of the octanol solvent in OPLS-AA, GAFF and CHARMM were validated by comparing computed against experimental values, namely the density as a function of temperature, the hydration free energy, the chemical potential, and the octanol-water partition coefficient. The partition coefficients for the SAMPL6-logP compounds were calculated from the solvation free energy of compounds in water and pure (dry) octanol or wet octanol with 27 mol % water dissolved. We used 5-ns windowed alchemical free energy perturbation calculations to compute absolute solvation free energies with thermodynamic integration (TI) and the multistate Bennett acceptance ratio (MBAR) (from the ALCHEMLYB library) with uncorrelated samples from the MD simulations.

An important lesson was that an initial equilibration period can have a large effect on the accuracy and we introduced a new quantity, the *equilibration ratio* A_c, to assess equilibration of sets of alchemical λ windows. Discarding the first 1 ns of each 5-ns window as an equilibration phase improved the RMSE of the GAFF $\log P_{ow}$ predictions by up to 0.8 log units. The improved accuracy was due to improved convergence in the Coulomb FEP windows with the octanol solvent. Equilibration (and

sampling) of the octanol simulations appeared to be more demanding than the water simulations.

Overall, CGenFF gave the best prediction with RMSE 1.2 log units although only for a partial data set of eight compounds and with relatively low Pearson correlation coefficient. When considering all eleven compounds, GAFF gave a respectable RMSE of 1.5. The GAFF and OPLS-AA results displayed a systematic error where molecules were too hydrophobic whereas CGenFF appeared to be more balanced, at least on this small data set. For OPLS-AA this error is possibly related to undersolvation; for GAFF its origin remains speculative although both force fields are known to be underpolarized. Sufficient sampling appears to be especially important for the octanol simulations whereas the force field accuracy appears the remaining challenge for the hydration simulations. Thus, $\log P$ calculations represent a well-balanced challenge for moving the field of molecular simulations forward.

Acknowledgements The authors would like to thank David L. Mobley and Teresa Danielle Bergazin for useful discussions and sharing unpublished data.

References

1. Kramer W (2011) Transporters, Trojan horses and therapeutics: suitability of bile acid and peptide transporters for drug delivery. Biol Chem 392(1-2):77–94, DOI 10.1515/BC.2011.017
2. Leeson PD, Springthorpe B (2007) The influence of drug-like concepts on decision-making in medicinal chemistry. Nat Rev Drug Discov 6(11):881–90, DOI 10.1038/nrd2445
3. Lipinski CA, Lombardo F, Dominy BW, Feeney PJ (1997) Experimental and computational approaches to estimate solubility and permeability in drug discovery and development settings. Advanced Drug Delivery Reviews 23(1):3–25.1, DOI 10.1016/S0169-409X(96)00423-1
4. Bannan CC, Burley KH, Chiu M, Shirts MR, Gilson MK, Mobley DL (2016) Blind prediction of cyclohexane–water distribution coefficients from the SAMPL5 challenge. Journal of Computer-Aided Molecular Design 30(11):927–944, DOI 10.1007/s10822-016-9954-8
5. Işık M, Levorse D, Mobley DL, Rhodes T, Chodera JD (2020) Octanol-water partition coefficient measurements for the SAMPL6 blind prediction challenge. J Comput Aided Mol Des (this issue), DOI 10.1007/s10822-019-00271-3
6. Beckstein O, Iorga BI (2012) Prediction of hydration free energies for aliphatic and aromatic chloro derivatives using molecular dynamics simulations with the OPLS-AA force field. J Comput Aided Mol Des 26(5):635–645, DOI 10.1007/s10822-011-9527-9
7. Beckstein O, Fourrier A, Iorga BI (2014) Prediction of hydration free energies for the SAMPL4 diverse set of compounds using molecular dynamics simulations with the OPLS-AA force field. J Comput Aided Mol Des 28(3):265–276, DOI 10.1007/s10822-014-9727-1

8. Kenney IM, Beckstein O, Iorga BI (2016) Prediction of cyclohexane-water distribution coefficients for the SAMPL5 data set using molecular dynamics simulations with the OPLS-AA force field. J Comput Aided Mol Des 30(11):1045–1058, DOI 10.1007/s10822-016-9949-5
9. Selwa E, Kenney IM, Beckstein O, Iorga BI (2018) SAMPL6: calculation of macroscopic pKa values from ab initio quantum mechanical free energies. Journal of Computer-Aided Molecular Design 32(10):1203–1216, DOI 10.1007/s10822-018-0138-6, URL `http://link.springer.com/10.1007/s10822-018-0138-6`
10. Işık M, Levorse D, Rustenburg AS, Ndukwe IE, Wang H, Wang X, Reibarkh M, Martin GE, Makarov AA, Mobley DL, Rhodes T, Chodera JD (2018) pKa measurements for the SAMPL6 prediction challenge for a set of kinase inhibitor-like fragments. J Comput Aided Mol Des 32(10):1117–1138, DOI 10.1007/s10822-018-0168-0
11. Frisch MJ, Trucks GW, Schlegel HB, Scuseria GE, Robb MA, Cheeseman JR, Scalmani G, Barone V, Mennucci B, Petersson GA, Nakatsuji H, Caricato M, Li X, Hratchian HP, Izmaylov AF, Bloino J, Zheng G, Sonnenberg JL, Hada M, Ehara M, Toyota K, Fukuda R, Hasegawa J, Ishida M, Nakajima T, Honda Y, Kitao O, Nakai H, Vreven T, Montgomery JA Jr, Peralta JE, Ogliaro F, Bearpark M, Heyd JJ, Brothers E, Kudin KN, Staroverov VN, Kobayashi R, Normand J, Raghavachari K, Rendell A, Burant JC, Iyengar SS, Tomasi J, Cossi M, Rega N, Millam JM, Klene M, Knox JE, Cross JB, Bakken V, Adamo C, Jaramillo J, Gomperts R, Stratmann RE, Yazyev O, Austin AJ, Cammi R, Pomelli C, Ochterski JW, Martin RL, Morokuma K, Zakrzewski VG, Voth GA, Salvador P, Dannenberg JJ, Dapprich S, Daniels AD, Farkas O, Foresman JB, Ortiz JV, Cioslowski J, Fox DJ (2009) Gaussian 09 Revision D.01. Gaussian Inc. Wallingford CT
12. Kaminski G, Duffy E, Matsui T, Jorgensen W (1994) Free energies of hydration and pure liquid properties of hydrocarbons from the OPLS all-atom model. J Phys Chem 98(49):13,077–13,082, DOI 10.1021/j100100a043
13. Jorgensen WL, Maxwell DS, Tirado-Rives J (1996) Development and testing of the OPLS all-atom force field on conformational energetics and properties of organic liquids. J Am Chem Soc 118(45):11,225–11,236, DOI 10.1021/ja9621760
14. Damm W, Frontera A, Tirado-Rives J, Jorgensen W (1997) OPLS all-atom force field for carbohydrates. J Comput Chem 18(16):1955–1970, DOI 10.1002/(SICI)1096-987X(199712)18:16<1955::AID-JCC1>3.0.CO;2-L
15. Jorgensen WL, McDonald NA (1998) Development of an all-atom force field for heterocycles. Properties of liquid pyridine and diazenes. J Mol Struct THEOCHEM 424(1-2):145–155, DOI 10.1016/S0166-1280(97)00237-6
16. McDonald NA, Jorgensen WL (1998) Development of an all-atom force field for heterocycles. Properties of liquid pyrrole, furan, diazoles, and oxazoles. J Phys Chem B 102(41):8049–8059, DOI 10.1021/jp981200o
17. Rizzo RC, Jorgensen WL (1999) OPLS all-atom model for amines: Resolution of the amine hydration problem. J Am Chem Soc 121(20):4827–4836, DOI 10.1021/ja984106u

18. Kaminski GA, Friesner RA, Tirado-Rives J, Jorgensen WL (2001) Evaluation and reparametrization of the OPLS-AA force field for proteins via comparison with accurate quantum chemical calculations on peptides. J Phys Chem B 105(28):6474–6487, DOI 10.1021/jp003919d
19. Dodda LS, Cabeza de Vaca I, Tirado-Rives J, Jorgensen WL (2017) LigParGen web server: an automatic OPLS-AA parameter generator for organic ligands. Nucleic Acids Res 45(W1):W331–W336, DOI 10.1093/nar/gkx312
20. Vanommeslaeghe K, Hatcher E, Acharya C, Kundu S, Zhong S, Shim J, Darian E, Guvench O, Lopes P, Vorobyov I, Mackerell AD Jr (2010) CHARMM general force field: A force field for drug-like molecules compatible with the CHARMM all-atom additive biological force fields. J Comput Chem 31(4):671–90, DOI 10.1002/jcc.21367
21. Vanommeslaeghe K, Raman EP, MacKerell AD (2012) Automation of the CHARMM General Force Field (CGenFF) II: Assignment of bonded parameters and partial atomic charges. Journal of Chemical Information and Modeling 52(12):3155–3168, DOI 10.1021/ci3003649
22. Vanommeslaeghe K, MacKerell AD (2012) Automation of the CHARMM General Force Field (CGenFF) I: bond perception and atom typing. Journal of Chemical Information and Modeling 52(12):3144–3154, DOI 10.1021/ci300363c
23. Soteras Gutiérrez I, Lin FY, Vanommeslaeghe K, Lemkul JA, Armacost KA, Brooks CL, MacKerell AD (2016) Parametrization of Halogen Bonds in the CHARMM General Force Field: Improved treatment of ligand-protein interactions. Bioorganic & medicinal chemistry 24(20):4812–4825, DOI 10.1016/j.bmc.2016.06.034
24. Wang J, Wolf RM, Caldwell JW, Kollman PA, Case DA (2004) Development and testing of a general AMBER force field. J Comput Chem 25(9):1157–74, DOI 10.1002/jcc.20035
25. Sousa da Silva AW, Vranken WF (2012) ACPYPE - AnteChamber PYthon Parser interfacE. BMC Res Notes 5:367, DOI 10.1186/1756-0500-5-367
26. Jorgensen WL, Chandrasekhar J, Madura JD, Impey RW, Klein ML (1983) Comparison of simple potential functions for simulating liquid water. J Chem Phys 79(2):926–935, DOI 10.1063/1.445869
27. Huang J, MacKerell AD Jr (2013) CHARMM36 all-atom additive protein force field: validation based on comparison to NMR data. J Comput Chem 34(25):2135–45, DOI 10.1002/jcc.23354
28. Maier JA, Martinez C, Kasavajhala K, Wickstrom L, Hauser KE, Simmerling C (2015) ff14SB: Improving the accuracy of protein side chain and backbone parameters from ff99SB. J Chem Theory Comput 11(8):3696–713, DOI 10.1021/acs.jctc.5b00255
29. Price DJ, Brooks CL 3rd (2004) A modified TIP3P water potential for simulation with Ewald summation. J Chem Phys 121(20):10,096–103, DOI 10.1063/1.1808117
30. Šegatin N, Klofutar C (2004) Thermodynamics of the Solubility of Water in 1-Hexanol, 1-Octanol, 1-Decanol, and Cyclohexanol. Monatshefte für Chemie / Chemical Monthly 135(3):241–248, DOI 10.1007/s00706-003-0053-x, URL `https://doi.org/10.1007/s00706-003-0053-x`

31. Lang BE (2012) Solubility of Water in Octan-1-ol from (275 to 369) K. Journal of Chemical & Engineering Data 57(8):2221–2226, DOI 10.1021/je3001427, URL https://doi.org/10.1021/je3001427
32. Cumming H, Rücker C (2017) Octanol–Water Partition Coefficient Measurement by a Simple 1H NMR Method. ACS Omega 2(9):6244–6249, DOI 10.1021/acsomega.7b01102, URL https://doi.org/10.1021/acsomega.7b01102
33. Abraham MJ, Murtola T, Schulz R, Páll S, Smith JC, Hess B, Lindahl E (2015) GROMACS: High performance molecular simulations through multi-level parallelism from laptops to supercomputers. SoftwareX 1–2:19 – 25, DOI 10.1016/j.softx.2015.06.001
34. Shirts MR, Chodera JD (2008) Statistically optimal analysis of samples from multiple equilibrium states. J Chem Phys 129(12):124,105, DOI 10.1063/1.2978177
35. Dotson D, Beckstein O, Wille D, Kenney I, shuail, trje3733, Lee H, Lim V, brycestx, Barhaghi MS (2019) alchemistry/alchemlyb: 0.3.0. Software, DOI 10.5281/zenodo.3361016, URL https://doi.org/10.5281/zenodo.3361016
36. Mobley DL, Dumont E, Chodera JD, Dill KA (2007) Comparison of charge models for fixed-charge force fields: Small-molecule hydration free energies in explicit solvent. J Phys Chem B 111(9):2242–2254, DOI 10.1021/jp0667442
37. Parrinello M, Rahman A (1981) Polymorphic transitions in single crystals: A new molecular dynamics method. J Appl Phys 52(12):7182–7190, DOI 10.1063/1.328693, URL http://link.aip.org/link/?JAP/52/7182/1
38. Shirts MR, Pitera JW, Swope WC, Pande VS (2003) Extremely precise free energy calculations of amino acid side chain analogs: Comparison of common molecular mechanics force fields for proteins. J Chem Phys 119(11):5740–5761, DOI 10.1063/1.1587119
39. Essman U, Perela L, Berkowitz ML, Darden T, Lee H, Pedersen LG (1995) A smooth particle mesh Ewald method. J Chem Phys 103:8577–8592, DOI 10.1063/1.470117
40. Hess B (2008) P-LINCS: A parallel linear constraint solver for molecular simulation. J Chem Theory Comput 4(1):116–122, DOI 10.1021/ct700200b
41. Hess B, Kutzner C, van der Spoel D, Lindahl E (2008) GROMACS 4: Algorithms for highly efficient, load-balanced, and scalable molecular simulation. J Chem Theory Comput 4(3):435–447, DOI 10.1021/ct700301q
42. Páll S, Abraham MJ, Kutzner C, Hess B, Lindahl E (2015) Tackling exascale software challenges in molecular dynamics simulations with GROMACS. In: Markidis S, Laure E (eds) Solving Software Challenges for Exascale: International Conference on Exascale Applications and Software, EASC 2014, Stockholm, Sweden, April 2-3, 2014, Revised Selected Papers, Lecture Notes in Computer Science, vol 8759, Springer International Publishing, Switzerland, pp 3–27, DOI 10.1007/978-3-319-15976-8_1
43. Klimovich PV, Shirts MR, Mobley DL (2015) Guidelines for the analysis of free energy calculations. J Comput Aided Mol Des 29(5):397–411, DOI 10.1007/s10822-015-9840-9

44. Chodera JD (2016) A simple method for automated equilibration detection in molecular simulations. J Chem Theory Comput 12(4):1799–1805, DOI 10.1021/acs.jctc.5b00784
45. Jorge M, Garrido N, Queimada A, Economou I, Macedo E (2010) Effect of the integration method on the accuracy and computational efficiency of free energy calculations using thermodynamic integration. J Chem Theory Comput 6(4):1018–1027, DOI 10.1021/ct900661c
46. Virtanen P, Gommers R, Oliphant TE, Haberland M, Reddy T, Cournapeau D, Burovski E, Peterson P, Weckesser W, Bright J, van der Walt SJ, Brett M, Wilson J, Millman KJ, Mayorov N, Nelson ARJ, Jones E, Kern R, Larson E, Carey C, Polat I, Feng Y, Moore EW, VanderPlas J, Laxalde D, Perktold J, Cimrman R, Henriksen I, Quintero EA, Harris CR, Archibald AM, Ribeiro AH, Pedregosa F, van Mulbregt P, SciPy 1·0 Contributors (2019) Scipy 1.0—fundamental algorithms for scientific computing in Python. arXiv 1907.10121v1
47. Faber NKM (1999) Estimating the uncertainty in estimates of root mean square error of prediction: application to determining the size of an adequate test set in multivariate calibration. Chemometrics and Intelligent Laboratory Systems 49(1):79 – 89, DOI 10.1016/S0169-7439(99)00027-1
48. Zangi R (2018) Refinement of the OPLSAA Force-Field for Liquid Alcohols. ACS Omega 3(12):18,089–18,099, DOI 10.1021/acsomega.8b03132
49. Işık M, Bergazin TD, Fox T, Rizzi A, Chodera JD, Mobley DL (2020) Assessing the accuracy of octanol-water partition coefficient predictions in the SAMPL6 Part II log P challenge. J Comput Aided Mol Des (this issue)
50. Yang W, Bitetti-Putzer R, Karplus M (2004) Free energy simulations: Use of reverse cumulative averaging to determine the equilibrated region and the time required for convergence. J Chem Phys 120(6):2618–2628, DOI 10.1063/1.1638996
51. Paranahewage SS, Gierhart CS, Fennell CJ (2016) Predicting water-to-cyclohexane partitioning of the SAMPL5 molecules using dielectric balancing of force fields. Journal of Computer-Aided Molecular Design 30(11):1059–1065, DOI 10.1007/s10822-016-9950-z, URL `https://doi.org/10.1007/s10822-016-9950-z`
52. Brini E, Fennell CJ, Fernandez-Serra M, Hribar-Lee B, Lukšič M, Dill KA (2017) How water's properties are encoded in its molecular structure and energies. Chemical Reviews 117(19):12,385–12,414, DOI 10.1021/acs.chemrev.7b00259
53. Swope WC, Horn HW, Rice JE (2010) Accounting for polarization cost when using fixed charge force fields. II. Method and application for computing effect of polarization cost on free energy of hydration. The Journal of Physical Chemistry B 114(26):8631–8645, DOI 10.1021/jp911701h
54. Lundborg M, Lindahl E (2015) Automatic gromacs topology generation and comparisons of force fields for solvation free energy calculations. J Phys Chem B 119(3):810–23, DOI 10.1021/jp505332p

Journal of Computer-Aided Molecular Design manuscript No.
(will be inserted by the editor)

Electronic supplementary material

Prediction of octanol-water partition coefficients for the SAMPL6-log P molecules using molecular dynamics simulations with OPLS-AA, AMBER and CHARMM force fields

Shujie Fan · Bogdan I. Iorga · Oliver Beckstein

Received: 16 October 2019 / Accepted: 27 November 2019

1 Solvent validation

The parametrization of octanol was validated by computing the density as a function of temperature, $\rho(T)$, from MD simulations and comparison to experimental densities. Table S1 explicitly lists the computed values and compared to an average over different experimental values. The relative error to the experiment $\rho_{\mathrm{sim}}/\rho_{\mathrm{exp}} - 1$ was below 4% at 298 K and 323 K and below 6% at 373 K. The only exception was the density for wet octanol at 273 K with OPLS-AA, which increased by 11%, because the mixture undergoes a freezing transition.

2 Estimator comparison

In our previous work [1–3] we used the TI estimator in MDPOW to calculate free energies. With the recent 0.3.0 release of alchemlyb, this library has matured sufficiently for production use and we wanted to compare if the MDPOW-TI estimator and the ALCHEMLYB estimators gave comparable results.

S. Fan
Department of Physics, Arizona State University, P.O. Box 871504, Tempe, AZ 85287-1504, USA

B. I. Iorga
Institut de Chimie des Substances Naturelles, CNRS UPR 2301, Université Paris-Saclay, Labex LERMIT, 1 Avenue de la Terrasse, 91198 Gif-sur-Yvette, France
Tel.: +33 1 69 82 30 94
Fax: +33 1 69 07 72 47
E-mail: bogdan.iorga@cnrs.fr

O. Beckstein
Department of Physics and Center for Biological Physics, Arizona State University, P.O. Box 871504, Tempe, AZ 85287-1504, USA
Tel.: +1 480 727 9765
Fax: +1 480 965-4669
E-mail: oliver.beckstein@asu.edu

Table S1: Density of octanol as a function of temperature.

Parametrization	Octanol	T (K)	ρ_{exp} (g·cm^{-3}) [a]	ρ_{sim} (g·cm^{-3}) [b]	rel.error [c]
OPLS-AA	dry	273	0.8383(10)	0.8359(44)	-0.3
	dry	298	0.8220(10)	0.8080(49)	-1.7
	dry	323	0.8068(26)	0.7822(53)	-3.0
	dry	348	0.7862(1)	0.7556(60)	-3.9
	dry	373	0.7697(33)	0.7274(68)	-5.5
	wet	273	0.8383(10)		
	wet	298	0.8220(10)		
	wet	323	0.8068(26)		
	wet	348	0.7862(1)		
	wet	373	0.7697(33)		
GAFF	dry	273	0.8383(10)	0.8214(41)	-2.0
	dry	298	0.8220(10)	0.7989(46)	-2.8
	dry	323	0.8068(26)	0.7757(50)	-3.8
	dry	348	0.7862(1)	0.7515(56)	-4.4
	dry	373	0.7697(33)	0.7258(62)	-5.7
	wet	273	0.8383(10)		
	wet	298	0.8220(10)		
	wet	323	0.8068(26)		
	wet	348	0.7862(1)		
	wet	373	0.7697(33)		
CGenFF	dry	273	0.8383(10)	0.8040(61)	-4.1
	dry	298	0.8220(10)	0.7902(66)	-3.9
	dry	323	0.8068(26)	0.7772(71)	-3.7
	dry	348	0.7862(1)	0.7645(74)	-2.8
	dry	373	0.7697(33)	0.7460(70)	-3.1
	wet	273	0.8383(10)		
	wet	298	0.8220(10)		
	wet	323	0.8068(26)		
	wet	348	0.7862(1)		
	wet	373	0.7697(33)		

[a] Experimental density values for dry octanol were calculated by averaging the experimental values at the same temperature. Errors were estimated as the standard deviation of the mean. [b] The simulated density was calculated from $\rho = m/V$, where m was the total mass of the system and the volume V was the average volume of a 100 ns length simulation at the given temperature. The error was estimated from the error propagation $\Delta\rho = \frac{m\Delta V}{V^2}$ and represents one standard deviation from the mean. [c] The relative error to experiment was calculated as $\rho_{sim}/\rho_{exp} - 1$.

Figure S1 shows that all three estimators give similar values for the $\log P_{ow}$ when provided with all the data, i.e., without decorrelation preprocessing. The root mean square difference (RMSD) over the whole data set for two estimators A and B

$$\mathrm{RMSD}(A,B) = \sqrt{N^{-1}\sum_{i=1}^{N}\left(A[\log P_{ow}^{(i)}] - B[\log P_{ow}^{(i)}]\right)^2} \tag{S1}$$

should ideally be 0, thus indicating that the two estimators give exactly the same answer for each molecule. As shown in the annotations in Figure S1, the difference between the estimators is typically about 0.1 log units and only for the OPLS-AA (LigParGen) it rises to 0.21 when comparing MDPOW-TI to MBAR (Figure S1b).

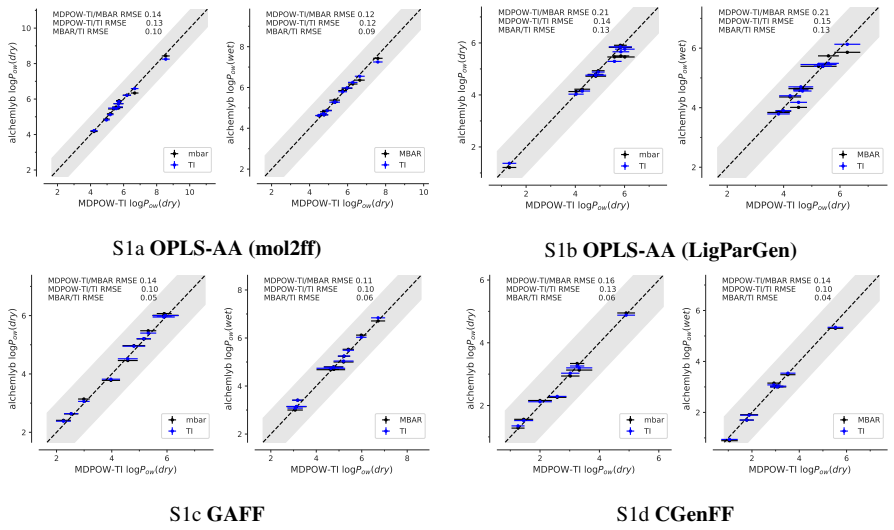

S1a **OPLS-AA (mol2ff)** S1b **OPLS-AA (LigParGen)**

S1c **GAFF** S1d **CGenFF**

Fig. S1: Comparison between the MDPOW-TI estimator and the ALCHEMLYB-TI or -MBAR estimators. Octanol-water coefficients $\log P_{ow}$ for simulations with dry or wet octanol were calculated with the MDPOW-TI estimator as in our previous work and compared to the ALCHEMLYB estimators. Data from all trajectory frames were used without any subsampling. The root mean square differences (RMSD) over the whole data set for the different combination of estimators are shown in the upper left hand corner. A value of 0 indicates that the two estimators give exactly the same answer for each molecule.

The major (expected) difference is that the MDPOW-TI estimator gives realistic error bars even when working with correlated data because it decorrelates data for its error estimation [1] (as seen in the figures) whereas ALCHEMLYB-TI and -MBAR require decorrelated data for their error estimates and produce unrealistically small error bars otherwise.

3 Analysis of convergence

Equations 15 and 16 in the main paper defined the "converged fraction" R_c of a FEP trajectory where $R_c = 0$ indicates that the whole trajectory can be used to estimate the free energy whereas $R_c = 1$ indicates that no parts of the trajectory are likely to give reliable estimates.

While the interpretation of $R_c = 0$ is clear, it might not be obvious that a high R_c reliably indicates poor convergence. Its value might fluctuate considerably because there is only one way in which a simulation can be converged but a multitude of ways in which it can fail to converge. Although we did not have independent statistical repeats to investigate the distribution of R_c for the same λ, anecdotal evidence such

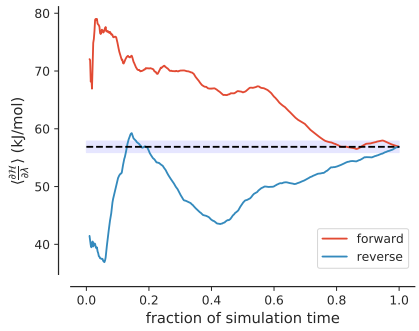

S2a octanol, $\lambda_{Coul} = 0$ and $\lambda_{vdW} = 0$

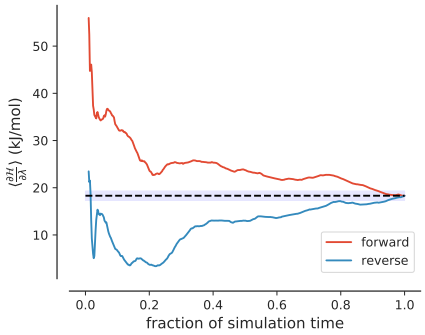

S2b octanol, $\lambda_{Coul} = 0.25$ and $\lambda_{vdW} = 0$

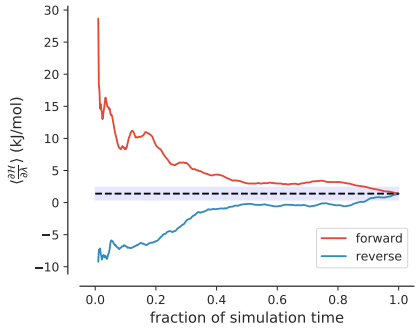

S2c octanol, $\lambda_{Coul} = 0.375$ and $\lambda_{vdW} = 0$

Fig. S2: $\left\langle \frac{\partial \mathscr{H}}{\partial \lambda} \right\rangle$ time-reversed and time-forward convergence plots for **SM14**. All of them showed poor convergence. S2a The calculated R_c is 0.95. S2b The calculated R_c is 0.92. S2c The calculated R_c is 0.93.

as the one in Fig. S2 for different λ windows showed that trajectories that converge poorly in different ways all produce $R_c > 0.9$.

3.1 Analysis of all simulations for all force fields

Similar to the results for **SM14** in the main paper, the cumulative distributions of the convergence time fractions $\mathscr{C}(R_c)$ of all Coulomb and VDW windows for all molecules from the whole data (all data, 0–5 ns) with OPLS-AA, LigParGen, GAFF and CGenFF parameters showed that the water simulations equilibrated much faster than the dry and the wet octanol simulations (Figure S3). No obvious improvement in the reduced data was observed in OPLS-AA (mol2ff), GAFF and CGenFF results. For OPLS-AA (LigParGen), discarding data worsened equilibration for Coulomb windows for water simulations and improved equilibration for Coulomb windows for dry and wet octanol windows.

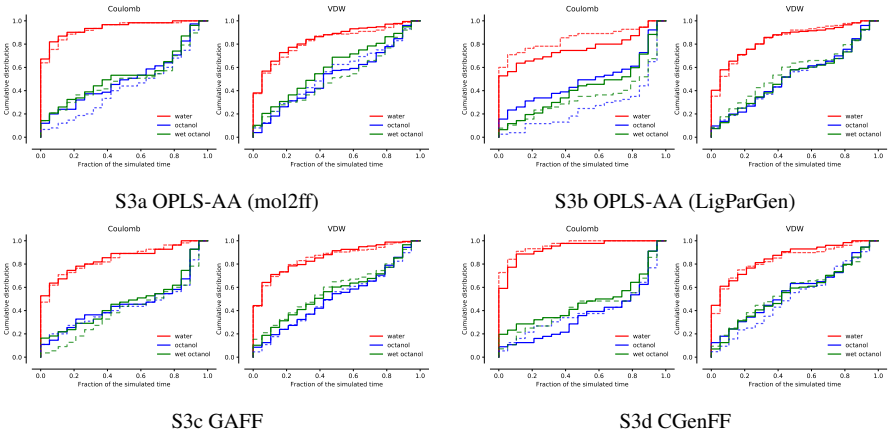

S3a OPLS-AA (mol2ff) S3b OPLS-AA (LigParGen)

S3c GAFF S3d CGenFF

Fig. S3: Cumulative distribution functions $\mathscr{C}(R_c)$ of R_c for Coulomb and VDW λ windows from all data (0–5 ns) (dashed lines) and data with the first 1 ns discarded as equilibration (1–5 ns) (solid lines) for all molecules with OPLS-AA (mol2ff), OPLS-AA (LigParGen), GAFF and CGenFF parameters.

To quantify the difference, we calculated the overall equilibrated ratios A_c of all Coulomb and VDW windows for all molecules from both all data and reduced data for all parameters (Table S2). Discarding the first 1 ns slightly improved the equilibration of Coulomb windows for OPLS-AA (mol2ff) and GAFF. Corresponding to the cumulative distributions of LigParGen results, the equilibrated ratio decreased by 0.09 for the 1–5 ns data for Coulomb windows of water simulations and increased by 0.22 and 0.07 for the 1–5 ns data for dry and wet octanol simulations. There was no overall trend or difference larger than 0.05 observed in CGenFF results.

Table S2: Overall equilibrated ratio A_c of all data (0–5 ns) and reduced data (1–5 ns) Coulomb and VDW windows of all data and reduced data for all molecules.

Parametrization	data set	Water		*Dry* Octanol		*Wet* Octanol	
		Coulomb	VDW	Coulomb	VDW	Coulomb	VDW
OPLS-AA	0–5 ns	0.93	0.82	0.43	0.55	0.50	0.51
OPLS-AA	1–5 ns	0.94	0.84	0.50	0.52	0.53	0.60
LigParGen	0–5 ns	0.85	0.84	0.27	0.51	0.35	0.56
LigParGen	1–5 ns	0.76	0.84	0.49	0.52	0.42	0.52
GAFF	0–5 ns	0.84	0.85	0.44	0.51	0.40	0.58
GAFF	1–5 ns	0.85	0.86	0.46	0.51	0.47	0.56
CHARMM	0–5 ns	0.96	0.84	0.39	0.51	0.44	0.57
CHARMM	1–5 ns	0.94	0.86	0.37	0.56	0.48	0.55

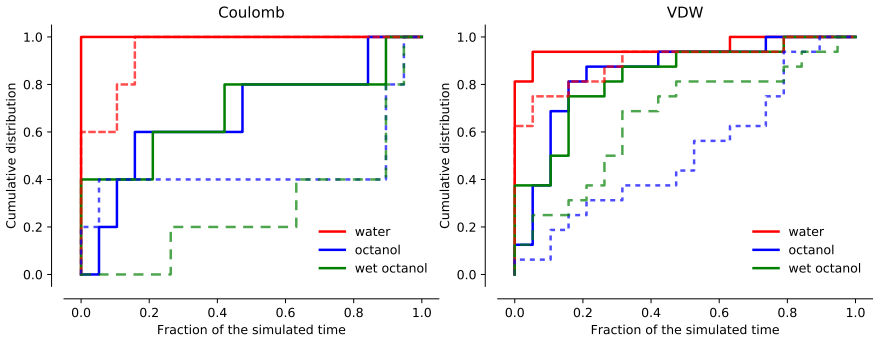

Fig. S4: Cumulative distribution functions $\mathscr{C}(R_c)$ of R_c for Coulomb and VDW λ windows from all data (0–5 ns) (dashed lines) and long simulation data (0–50 ns) (solid lines) for **SM14** (GAFF)

3.2 Comparison with long simulation time protocol

To test whether A_c could well describe the equilibration of the simulations, we ran FEP simulations for **SM14** (GAFF) using a protocol with a 100 ns NPT equilibrium simulation and 50 ns production simulations. As shown in Figure S4, the water simulations equilibrated much faster than the dry and the wet octanol simulations in both Coulomb and VDW parts for 0–50 ns data, the same as the 0–5 ns data. A_c of dry and wet octanol simulations for 0–50 ns data showed an overall improvement from 0.17 to 0.42 (Table S3), corresponding to the intuition that longer simulations improved the equilibrated fraction of the simulations. Removing the first nanosecond from the 50-ns windows ("1–50 ns") did not improve the equilibration behavior as measured by A_c as seen in Table S3, possibly because that part of the trajectory only contributed 1/50 to the total.

The computed $\log P_{ow}$ values for **SM14** with 0–50-ns windows were 3.08 ± 0.08 (dry) and 3.09 ± 0.07 (wet). With discarding the first nanoseconds, these values became 2.78 ± 0.07 (dry) and 2.98 ± 0.07 (wet). These numbers agreed less with the experimental reference value (1.95 ± 0.03) than the calculated ones from the shorter

Table S3: Equilibrated ratio A_c of all data (0–5 ns, 1–5 ns) and long simulation data (0–50 ns, 1–50 ns) Coulomb and VDW windows of all data and reduced data for **SM14**.

	Water		*Dry* Octanol		*Wet* Octanol	
	Coulomb	VDW	Coulomb	VDW	Coulomb	VDW
0–5 ns	0.95	0.90	0.44	0.51	0.27	0.66
1–5 ns	0.95	0.93	0.51	0.57	0.54	0.58
0–50 ns	1.00	0.95	0.67	0.85	0.69	0.83
1–50 ns	1.00	0.95	0.68	0.84	0.68	0.83

simulations (2.32 ± 0.21 and 2.62 ± 0.26, see Table 6 in the main paper). However, this value agreed well with the value of 2.8 ± 0.2 by Işık *et al* [4] (presented in their Table 5), which they obtained for the same micro state **SM14_micro001** with their indirect solvation-based free energy (IFE) protocol in dry octanol and the GAFF force field (see also Section 7).

The statistical error estimates from the long uncorrelated data were smaller by approximately a factor of three compared to the shorter runs. This increase in accuracy indicated that relevant system configurations were sampled better, thus leading to a more consistent free energy estimate.

Both the A_c analysis and the decreased statistical errors indicated that the longer calculations were better sampled than the shorter ones. Therefore, the better agreement of the shorter simulations with experiments was fortuitous. Future work will need to pay close attention to equilibration and convergence of individual λ-windows. The A_c measure might provide a useful tool to decide how far individual FEP simulation windows would need to be extended to obtain satisfactory convergence, for example, as part of automated iterative FEP workflows.

4 Comparison of dry and wet octanol simulations

As mentioned in the *SAMPL6 log P Challenge Instructions* (`https://github.com/samplchallenges/SAMPL6/blob/master/logP_challenge_instructions.md`), the experiments were performed in a phase-separated water/octanol environment but after mixing, these might not any longer be pure phases. We assumed that the water phase remained pure without any octanol. For the octanol phase we considered the pure "dry" octanol phase and the "wet" octanol phase with a mole fraction of 0.2705 water in octanol at 298 K [5].

The difference in $\log P_{ow}$ between dry and wet simulations was generally within 1 log-unit, as shown in the correlation plots in Figure S5. As described in the main paper, we did not observe a systematic improvement in $\log P_{ow}$ prediction by using wet octanol over the pure phases.

5 Submitted SAMPL6 predictions

Our submitted predictions to the SAMPL6-logP challenge followed the protocol that we had established for previous SAMPL challenges [1–3]. As part of the post-analysis stage we implemented a number of improvements and "lessons learned" into our analysis workflow that improved the agreement between our results and the experimental values. In the main manuscript we discuss these improvements and primarily present what we consider our current best approach. For completeness, we show the originally submitted data in Tables S4–S7 together with the SAMPL6 submission IDs and RMSE, AUE, and ME compared to the experimental values.

Table S4: **OPLS-AA (mol2ff)** $\log P_{ow}$ results submitted as entries **cp8kv** (Protocol *Dry*) and **623c0** (Protocol *Wet*), and experimental $\log P_{ow}$ with error estimate.

id	Exp.	Protocol *Dry*[a]		Protocol *Wet*	
	$\log P_{ow}^{\text{exp}}$	$\log P_{ow}$	Δ	$\log P_{ow}$	Δ
SM02	4.09(3)	5.69(30)	1.60(30)	5.74(23)	1.65(23)
SM04	3.98(3)	6.67(23)	2.69(23)	6.64(26)	2.66(26)
SM07	3.21(4)	5.19(20)	1.98(20)	4.73(18)	1.52(18)
SM08	3.1(3)	8.55(24)	5.45(24)	7.59(25)	4.49(25)
SM09	3.03(7)	5.69(27)	2.66(27)	4.92(25)	1.89(25)
SM11	2.1(4)	4.96(20)	2.86(20)	4.76(22)	2.66(22)
SM12	3.83(3)	6.2(25)	2.37(25)	5.97(28)	2.14(28)
SM13	2.92(4)	5.55(25)	2.63(25)	5.32(28)	2.40(28)
SM14	1.95(3)	4.21(22)	2.26(22)	4.49(18)	2.54(18)
SM15	3.07(3)	5.72(18)	2.65(18)	5.33(17)	2.26(17)
SM16	2.62(1)	5.4(34)	2.78(34)	6.27(25)	3.65(25)
RMS Error (RMSE)			2.88(7)		2.67(7)
Absolute Unsigned Error (AUE)			2.72(7)		2.53(7)
Mean Error (ME)			2.72(7)		2.53(7)

The difference Δ between experimental and computed octanol-water distribution coefficients is shown for each compound. The standard error of the mean in the last significant digits is given in parentheses. The root mean square error (RMSE), the absolute unsigned error (AUE), and the signed mean error (ME) were calculated as described in the Methods in the main paper.

Table S5: **OPLS-AA (LigParGen)** $\log P_{ow}$ results submitted as entries **eufcy** (Protocol *Dry*) and **mwuua** (Protocol *Wet*), and experimental $\log P_{ow}$ with error estimate.

id	Exp.	Protocol *Dry*		Protocol *Wet*	
	$\log P_{ow}^{\text{exp}}$	$\log P_{ow}$	Δ	$\log P_{ow}$	Δ
SM02	4.09(3)	6.01(40)	1.92(40)	6.26(46)	2.17(46)
SM04	3.98(3)	5.85(34)	1.87(34)	5.39(32)	1.41(32)
SM07	3.21(4)	4.93(26)	1.72(26)	4.53(30)	1.32(30)
SM08	3.1(3)	5.59(28)	2.49(29)	5.59(37)	2.49(37)
SM09	3.03(7)	4.83(42)	1.80(42)	5.24(64)	2.21(64)
SM11	2.1(4)	4.82(32)	2.72(32)	4.61(27)	2.51(27)
SM12	3.83(3)	5.83(26)	2.00(26)	4.61(44)	0.78(44)
SM13	2.92(4)	5.83(47)	2.91(47)	4.23(39)	1.31(39)
SM14	1.95(3)	1.32(28)	−0.63(28)	3.82(40)	1.87(40)
SM15	3.07(3)	4.03(31)	0.96(31)	3.99(28)	0.92(28)
SM16	2.62(1)	4.28(32)	1.66(32)	4.67(32)	2.05(32)
RMS Error (RMSE)			1.99(10)		1.83(12)
Absolute Unsigned Error (AUE)			1.88(10)		1.73(11)
Mean Error (ME)			1.77(10)		1.73(11)

Table S6: **GAFF** $\log P_{ow}$ results submitted as entries **sqosi** (Protocol *Dry*) and **6nmtt** (Protocol *Wet*), and experimental $\log P_{ow}$ with error estimate.

id	Exp.	Protocol *Dry*		Protocol *Wet*	
	$\log P_{ow}^{\text{exp}}$	$\log P_{ow}$	Δ	$\log P_{ow}$	Δ
SM02	4.09(3)	5.32(28)	1.23(29)	5.41(25)	1.32(25)
SM04	3.98(3)	5.9(27)	1.92(27)	5.98(23)	2.00(23)
SM07	3.21(4)	4.8(41)	1.59(41)	5.2(44)	1.99(44)
SM08	3.1(3)	5.88(40)	2.78(40)	4.77(23)	1.67(23)
SM09	3.03(7)	3.97(33)	0.94(33)	4.76(43)	1.73(43)
SM11	2.1(4)	2.25(27)	0.15(27)	3.18(24)	1.08(24)
SM12	3.83(3)	5.16(26)	1.33(26)	5.22(27)	1.39(27)
SM13	2.92(4)	5.95(47)	3.03(47)	6.72(31)	3.80(31)
SM14	1.95(3)	2.53(26)	0.58(26)	3.07(34)	1.12(34)
SM15	3.07(3)	2.99(21)	−0.08(21)	3.13(44)	0.06(44)
SM16	2.62(1)	4.58(36)	1.96(36)	4.64(63)	2.02(63)
RMS Error (RMSE)			1.69(11)		1.87(11)
Absolute Unsigned Error (AUE)			1.42(10)		1.65(11)
Mean Error (ME)			1.42(10)		1.65(11)

Table S7: **CGenFF** $\log P_{ow}$ results submitted as entry **3oqhx** for Protocol *Dry* (Protocol *Wet* was not submitted), and experimental $\log P_{ow}$ with error estimate.

id	Exp.	Protocol *Dry*		Protocol *Wet*	
	$\log P_{ow}^{\text{exp}}$	$\log P_{ow}$	Δ	$\log P_{ow}$	Δ
SM02	4.09(3)	2.54(51)	−1.55(51)	1.85(21)	−2.24(21)
SM04	3.98(3)	0.0(1000)	−3.98(1000)	0.0(1000)	−3.98(1000)
SM07	3.21(4)	4.08(38)	0.87(38)	−6.84(19)	−10.05(19)
SM08	3.1(3)	3.62(100)	0.52(100)	−9.54(96)	−12.64(96)
SM09	3.03(7)	0.2(134)	−2.83(134)	−9.54(122)	−12.57(122)
SM11	2.1(4)	2.42(34)	0.32(34)	−6.94(1000)	−9.04(1000)
SM12	3.83(3)	0.0(1000)	−3.83(1000)	0.0(1000)	−3.83(1000)
SM13	2.92(4)	4.16(56)	1.24(57)	−7.76(1000)	−10.68(1000)
SM14	1.95(3)	1.93(39)	−0.02(39)	0.0(0)	−1.95(3)
SM15	3.07(3)	2.79(36)	−0.28(36)	0.0(0)	−3.07(3)
SM16	2.62(1)	0.0(1000)	−2.62(1000)	0.0(1000)	−2.62(1000)
RMS Error (RMSE)			1.06(8)		1.30(10)
Absolute Unsigned Error (AUE)			0.83(9)		0.94(9)
Mean Error (ME)			−0.21(9)		−0.08(9)

The compounds **SM04**, **SM12** and **SM16** contained halogens with lone pairs and could therefore not be processed with the `cgenff_charmm2gmx.py` script so that we were not able to obtain Gromacs CGenFF parameters. In the submitted results, we set the $\log P_{ow}$ for these compounds as 0 with an uncertainty of 10 log units.

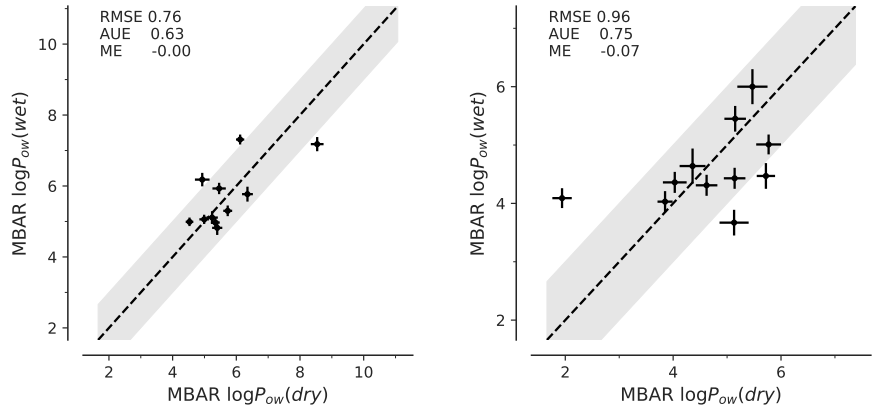

S5a **OPLS-AA (mol2ff)**

S5b **OPLS-AA (LigParGen)**

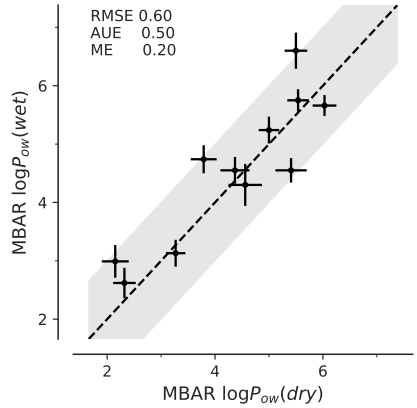

S5c **GAFF**

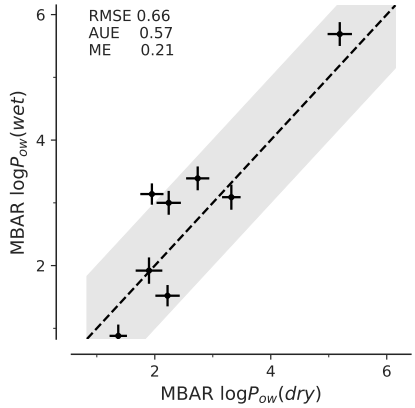

S5d **CGenFF**

Fig. S5: Correlation between octanol-water partition coefficients $\log P_{ow}$ computed with dry or wet octanol. The dashed line indicates perfect correlation with the gray band at ± 1 $\log P_{ow}$-unit.

6 Statistics for the reduced data set

As discussed in the main paper, we did not compute $\log P_{ow}$ values for the Cl-containing compounds **SM04**, **SM12**, and **SM16** with CHARMM/CGenFF because the currently available version of the `cgenff_charmm2gmx.py` script for the conversion of the CGenFF server files in CHARMM format to Gromacs format did not support lone pairs that are required for some halogen-containing compounds. Therefore, CGenFF results were only available for a reduced data set of the eight compounds **SM02**, **SM07**, **SM08**, **SM09**, **SM11**, **SM13**, **SM14**, and **SM15**. In Table S8 we computed the summary statistics for all force fields over this reduced data set. The

statistics for OPLS-AA (mol2ff), OPLS-AA (LigParGen), and GAFF for the reduced data set were not substantially different from the values over the whole data set and thus omitting the three compounds would not dramatically change any of our conclusions. Therefore, we chose to discuss the CGenFF results (eight compounds) together with the other three parametrizations (eleven compounds) on equal footing, assuming that the lower count of samples for CGenFF would not dramatically distort the comparison.

7 Comparison with data from Ref. [4]

Mobley and colleagues performed alchemical free energy calculations as reference calculations, including simulations with dry and wet octanol with the GAFF force field and TIP3P water model [4]. Their calculations **REF07** (dry) and **REF02** (wet) used a direct transfer free energy protocol whereas their simulation **IFE** (dry) used an indirect solvation-free energy based method that is similar to the approach taken in this work.

As shown in Fig. S6, the two approaches gave substantially different values, with the root mean square difference (RMSD, which was calculated in the same way as the RMSE) between the two different approaches consistently greater than 2 (dry **sqosi/REF07** 2.28 and **sqosi/IFE** 2.38; wet **6nmtt/REF02** 2.40). The main differences between these simulations were that our work used different tautomers for some of the molecules, the reference calculations **REF02** and **REF07** assigned partial charges to the carboxylic acid of **SM08** inappropriately, and the reference calculations included a much longer equilibration phase for the octanol simulations (500 ns) [4]. As discussed in detail by Işık *et al* [4], partial charge assignment made a large difference on a per molecule basis. However, across the data set, the difference in octanol equilibration period appeared to be dominating the difference between the methods. Our finding that longer sampling of our **SM14_micro001** with GAFF

Table S8: *RMSE*, *AUE* and *ME* of results for the eight compounds **SM02**, **SM07**, **SM08**, **SM09**, **SM11**, **SM13**, **SM14**, **SM15**, which could be parameterized with CGenFF. Data were taken from 1–5 ns (0–1 ns was discarded as equilibration), decorrelated, and processed with MBAR.

parameter	octanol	RMSE	AUE	ME
OPLS-AA	dry	2.94(5)	2.72(5)	2.72(5)
OPLS-AA	wet	2.60(5)	2.49(5)	2.49(5)
LigParGen	dry	1.71(6)	1.53(6)	1.52(6)
LigParGen	wet	1.74(6)	1.64(6)	1.64(6)
GAFF	dry	1.42(7)	1.11(7)	1.11(7)
GAFF	wet	1.75(8)	1.43(7)	1.43(7)
CGenFF	dry	1.17(5)	0.91(6)	−0.32(6)
CGenFF	wet	1.42(5)	1.05(5)	−0.10(5)

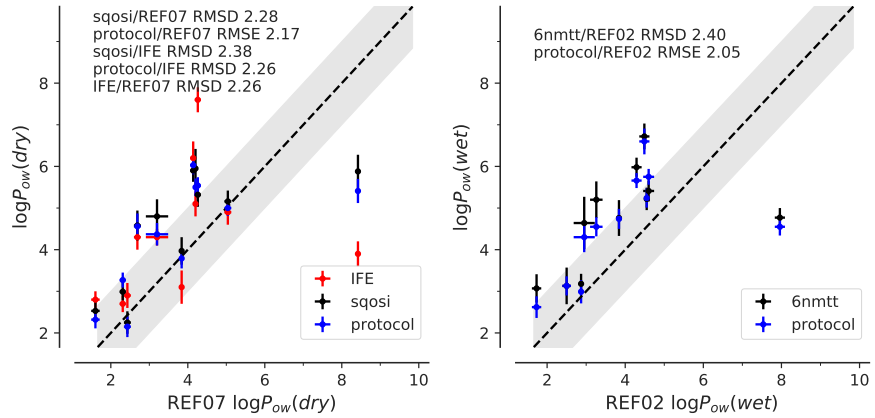

Fig. S6: Comparison of submitted GAFF results with reference calculations. Our original submissions **sqosi** and **6nmtt** as well as our improved protocol (labeled "protocol") were compared to the reference calculations in data from Ref. [4], namely the **REF07** and **REF02** data sets. The abscissa represents the reference calculations and the ordinate the calculations discussed in this work or data set **IFE**. The RMSD between data sets is shown in the inset. *Left*: dry octanol. *Right*: wet octanol.

and in dry octanol (see Section 3.2) reproduced their $\log P_{ow}$ value quantitatively [2.78 ± 0.07 (this work) *vs*. 2.8 ± 0.2 (Ref [4])] also corroborated the conclusion that sufficient sampling of the octanol solvent was an important difference between the two sets of simulations.

References

1. Beckstein O, Iorga BI (2012) Prediction of hydration free energies for aliphatic and aromatic chloro derivatives using molecular dynamics simulations with the OPLS-AA force field. J Comput Aided Mol Des 26(5):635–645, DOI 10.1007/s10822-011-9527-9
2. Beckstein O, Fourrier A, Iorga BI (2014) Prediction of hydration free energies for the SAMPL4 diverse set of compounds using molecular dynamics simulations with the OPLS-AA force field. J Comput Aided Mol Des 28(3):265–276, DOI 10.1007/s10822-014-9727-1
3. Kenney IM, Beckstein O, Iorga BI (2016) Prediction of cyclohexane-water distribution coefficients for the SAMPL5 data set using molecular dynamics simulations with the OPLS-AA force field. J Comput Aided Mol Des 30(11):1045–1058, DOI 10.1007/s10822-016-9949-5
4. Işık M, Bergazin TD, Fox T, Rizzi A, Chodera JD, Mobley DL (2020) Assessing the accuracy of octanol-water partition coefficient predictions in the SAMPL6 Part II log P challenge. J Comput Aided Mol Des (this issue)

5. Lang BE (2012) Solubility of Water in Octan-1-ol from (275 to 369) K. Journal of Chemical & Engineering Data 57(8):2221–2226, DOI 10.1021/je3001427, URL https://doi.org/10.1021/je3001427